Title:

Biosynthesis of gibberellin-related compounds modulates far-red light responses in the liverwort *Marchantia polymorpha*

Authors:

Rui Sun (孙 芮)[1], Maiko Okabe (岡部 麻衣子)[1], Sho Miyazaki (宮崎 翔)[2], Toshiaki Ishida (石田 俊晃)[3], Kiyoshi Mashiguchi (増口 潔)[3], Keisuke Inoue (井上 佳祐)[1], Yoshihiro Yoshitake (吉竹 良洋)[1], Shohei Yamaoka (山岡尚平)[1], Ryuichi Nishihama (西浜 竜一)[1,4], Hiroshi Kawaide (川出 洋)[5], Masatoshi Nakajima (中嶋 正敏)[6], Shinjiro Yamaguchi (山口 信次郎)[3], Takayuki Kohchi (河内 孝之)[1,*]

[1] Graduate School of Biostudies, Kyoto University, Kyoto 606-8502, Japan.

[2] Institute of Global Innovation Research, Tokyo University of Agriculture and Technology, Fuchu, 183-8509, Japan.

[3] Institute for Chemical Research, Kyoto University, Uji 611-0011, Japan.

[4] Department of Applied Biological Science, Faculty of Science and Technology, Tokyo University of Science, Noda 278-8510, Japan.

[5] Institute of Agriculture, Tokyo University of Agriculture and Technology, Tokyo 183-8509, Japan.

[6] Department of Applied Biological Chemistry, The University of Tokyo, Tokyo 113-8657, Japan.

[*] Correspondence: tkohchi@lif.kyoto-u.ac.jp

The author responsible for distribution of materials integral to the findings presented in this article in accordance with the policy described in the Instructions for Authors (https://academic.oup.com/plcell/pages/General-Instructions) is: Takayuki Kohchi (tkohchi@lif.kyoto-u.ac.jp).

25 **Short title:**

26 GA biosynthesis in *M. polymorpha*

27

ABSTRACT

The phytohormone gibberellins (GAs) are key regulators of growth, development and environmental responses in angiosperms. From an evolutionary perspective, all major steps of GA biosynthesis are conserved among vascular plants, while GA biosynthetic intermediates such as *ent*-kaurenoic acid (KA) are also produced by bryophytes. Here we show that in the liverwort *Marchantia polymorpha*, KA and GA_{12} are synthesized by evolutionarily conserved enzymes, which are required for developmental responses to far-red light (FR). Under FR-enriched conditions, mutants of various biosynthesis enzymes consistently altered thallus growth allometry, delayed the initiation of gametogenesis, and affected the morphology of gamete-bearing structures (gametangiophores). By chemical treatments and LC-MS/MS analyses, we confirmed these phenotypes were caused by deficiency of some GA-related compounds derived from KA, but not bioactive GAs from vascular plants. Transcriptome analysis showed that FR enrichment induced the up-regulation of genes related to stress responses and secondary metabolism in *M. polymorpha*, which was largely dependent on the biosynthesis of GA-related compounds. Due to the lack of the canonical GA receptors in bryophytes, we hypothesize that GA-related compounds are commonly synthesized in land plants but co-opted independently to regulate responses to light quality change in different lineages during the past 450 million years of evolution.

INTRODUCTION

Throughout evolution, plants developed various chemical tools to optimize growth and development, and to cope with environmental changes. Gibberellins (GAs) are a group of tetracyclic diterpenoid compounds broadly produced by many plants and plant-associated microbes. Among the more than 130 identified GAs, a few of them (GA_1, GA_3, GA_4, and GA_7) are considered as commonly bioactive in angiosperms (reviewed in Sponsel, 2016), stimulating seed germination (Koornneef and van der Veen, 1980; Toyomasu et al., 1998; Yamaguchi et al., 1998a; Ogawa et al., 2003; Gabriele et al., 2009) and promoting growth of various plant organs (Kurosawa, 1926; Koornneef and van der Veen, 1980; Wenzel et al., 2000; Ubeda-Tomás et al., 2008, 2009; Achard et al., 2009; Nelissen et al., 2012).

In *Arabidopsis thaliana*, the biosynthesis of GAs starts with the production of *ent*-kaurene from geranylgeranyl diphosphate (GGDP) by two terpene synthases (TPSs), *ent*-copalyl

diphosphate synthase (CPS) and *ent*-kaurene synthase (KS) (Sun and Kamiya, 1994; Yamaguchi et al., 1998b). Next, *ent*-kaurene is oxidized by two cytochrome P450 monooxygenases (CYPs), first into *ent*-kaurenoic acid (KA) by *ent*-kaurene oxidase (KO), then into GA_{12} by *ent*-kaurenoic acid oxidase (KAO) (Helliwell et al., 1998, 1999, 2001a, 2001b). Finally, GA_{12} is converted into the bioactive form GA_4 through sequential oxidation by two 2-oxoglutarate-dependent dioxygenases (2-OGDs), GA 20-oxidase (GA20ox) and GA 3-oxidase (GA3ox) (Chiang et al., 1995; Yamaguchi et al., 1998a; Williams et al., 1998). A second bioactive GA, GA_1, is different from GA_4 by one additional hydroxyl group on C-13, which is possibly introduced to GA_{12} or KA before the subsequent oxidation steps (Talon et al., 1990; Nomura et al., 2013) (Supplemental Figure 1).

Bioinformatic and chemical analyses revealed that this biosynthetic pathway producing GA_4 and/or GA_1 is conserved among vascular plants (Hirano et al., 2007; Tanaka et al., 2014; Cannell et al., 2020). In several fern species, GA-derived compounds modulate sexual differentiation of gametophytes and spore germination in the darkness (Yamane, 1998; Schneller, 2008; Tanaka et al., 2014; Hornych et al., 2021). Bryophytes have no 2-OGD-family members of GA biosynthesis enzymes, thus considered as lacking the production of common bioactive GAs. However, homologs for CPS, KS, KO and KAO still exist in bryophytes, which suggested an ancestral capacity to synthesize the GA precursors KA and GA_{12} in all land plants (Cannell et al., 2020). In the moss *Physcomitrium patens* which lacks KAO, KA is synthesized by a bifunctional CPS/KS and a single KO homolog (Hayashi et al., 2006, 2010; Miyazaki et al., 2011, 2015). The KA derivative, *ent*-3β-OH-KA, is known as a bioactive molecule to regulate protonema differentiation and blue light avoidance in *P. patens* (Hayashi et al., 2010; Miyazaki et al., 2014, 2015, 2018).

In the liverwort *Marchantia polymorpha*, homologs for CPS, KS, KO and KAO were identified in genome-wide analyses (Kumar et al., 2016; Bowman et al., 2017). Also, MpCPS/DTPS3 and MpKS/DTPS4 (hereafter referred to as MpCPS and MpKS) have been reported to catalyze the production of *ent*-copalyl diphosphate and *ent*-kaurene (Kumar et al., 2016; Jia et al., 2022). In transcriptome analysis, upregulation of GA biosynthesis gene homologs was observed under far-red light (FR) enriched conditions, suggesting a role for this pathway in the response to light quality change (Briginshaw et al., 2022). However, no empirical knowledge

has been established yet about the exact physiological function of GA-related compounds in liverworts.

FR enrichment mimics the proximity of competitive neighbors in the nature habitat. In many angiosperms, this is perceived by phytochrome (phy) photoreceptors and triggers shade-avoiding responses, including elongation of stem-like structures, hyponastic growth of petioles and acceleration of flowering (Downs et al., 1957; Holmes and Smith, 1975; Morgan and Smith, 1978, 1979; Whitelam and Johnson, 1982; Whitelam and Smith, 1991). GA biosynthesis is often evoked in this process, and is required for the induction of elongative growth (García-Martínez et al., 1987; Beall et al., 1996; Van Tuinen et al., 1999; Hisamatsu et al., 2005; Djakovic-Petrovic et al., 2007; Dubois et al., 2010). For example, in *A. thaliana*, a local FR enrichment at the leaf tip induced the expression of GA biosynthesis genes in both the leaf tip and the petiole, which modulates the hyponastic growth of the petiole (Sessa et al., 2005; Hisamatsu et al., 2005; Djakovic-Petrovic et al., 2007; Bou-Torrent et al., 2014; Kohnen et al., 2016; Küpers et al., 2023). In the gymnosperm *Pinus tabuliformis*, FR-induced shoot elongation was also accompanied with and dependent on the accumulation of bioactive GAs (Li et al., 2020).

As a liverwort, the life cycle of *M. polymorpha* is dominated by the thalloid gametophyte. End-of-day FR irradiation is known to cause hyponastic growth of thallus tips and decrease in chlorophyll (Fredericq, 1964; Ninnemann and Halbsguth, 1965; Fredericq and de Greef, 1966; Fredericq and Greef, 1968). FR enrichment also induced hyponastic thallus growth (Briginshaw et al., 2022), accompanied by the growth activity change of apical meristems and the transition to sexual reproduction (Chiyoda et al., 2008; Inoue et al., 2019; Streubel et al., 2023). Similar to *A. thaliana* and other land plants, these responses in *M. polymorpha* are mediated by the sole phytochrome (Mpphy) and the single-copy transcription factor PHYTOCHROME-INTERACTING FACTOR (MpPIF) (Fredericq, 1964; Inoue et al., 2016, 2019; Streubel et al., 2023). In this study, we characterized evolutionarily conserved GA biosynthesis enzymes in *M. polymorpha* with genetic approach, showing that they were indispensable for developmental and gene expression responses to FR enrichment.

118 **RESULTS**

119 **Mp*CPS* is required for thallus morphological changes induced by FR enrichment**

120 To explore the function of GA-related hormones in *M. polymorpha*, we used the
121 CRISPR/Cas9^{D10A} nickase system (Hisanaga et al., 2019; Koide et al., 2020) to create large-
122 deletion mutants of Mp*CPS* (Mp2g07200), which encodes the first enzyme of the biosynthesis
123 pathway. Two different mutant alleles (Mp*cps-4*^{ld} and Mp*cps-27*^{ld}) with complete loss of the
124 coding sequence (CDS) were isolated from Tak-1, a male wild-type accession (Supplemental
125 Figure 2A). Mp*cps-4*^{ld} was further complemented by expressing the CDS of Mp*CPS* with C-
126 terminal Citrine fusion under the control of a cauliflower mosaic virus 35S promoter
127 ($_{pro}$*35S:*Mp*CPS-Cit*), generating two independent transgenic lines. First, we observed the
128 thallus morphology of 12-day-old plants grown from gemmae under two different light
129 conditions, either the continuous white light (cW), or cW supplemented with continuous far-red
130 light (cW+cFR). FR enrichment under cW+cFR induced morphological changes in Tak-1 wild-
131 type plants, marked by increased growth angles (hyponasty) and slenderer thallus shapes, the
132 latter shown as the increase of length-width ratio measured from half of the thallus (Figure 1A-
133 C). Such an increase was not observed in Mp*cps*^{ld} mutants, suggesting a role for Mp*CPS* in
134 modulating FR-induced growth responses. Furthermore, Mp*cps*^{ld} mutants were significantly
135 larger in thallus size than wild-type plants, particularly under cW+cFR conditions (Figure 1A,D).
136 It is likely that MpCPS acts in a pathway producing compounds inhibiting growth, rather than
137 promoting growth like bioactive GAs in angiosperms. The complementation lines carrying
138 $_{pro}$*35S:*Mp*CPS-Cit* recovered the hyponastic growth, the thallus shape and the thallus size of
139 Mp*cps-4*^{ld}, confirming that the phenotypes were caused by Mp*CPS* loss-of-function (Figure 1A-
140 D). As a further verification, Mp*cps*^{ld} mutant alleles and complementation lines were
141 constructed in the female wild-type accession (Tak-2). Similarly, Mp*cps*^{ld} mutations resulted in
142 decrease of thallus hyponasty and the length-width ratio, but increased the thallus area
143 drastically under cW+cFR (Supplemental Figure 3).

144 To examine the influence of Mp*cps*^{ld} on growth activity at the tissue level, we labelled 7-day-
145 old plants grown under cW+cFR with 5-ethynyl-2'-deoxyuridine (EdU), which could be
146 incorporated into actively dividing cells during DNA synthesis. In the wild-type plants, we
147 observed a relatively narrow distribution of EdU-positive nuclei in the slender thallus,
148 dispersing from the apical meristem to the basal region along the midrib. By assigning different

149 pseudo-colors to signals acquired at different depths by confocal microscopy, we found
150 different distributions of dorsal and ventral signals in these plants. Ventral EdU signals along
151 the midrib extended further in the basal direction, suggesting excessive cell divisions specific
152 to the ventral side, which might contribute to the hyponastic growth induced by FR enrichment
153 (Figure 1E). While in Mp*cps*^{ld} mutants, EdU signals indicated active cell divisions in a broader
154 range. Two fully separated apical meristems were usually seen from the observed region, and
155 the total numbers of EdU-positive nuclei were significantly higher than those of wild-type plants
156 or complementation lines (Figure 1E-F). In addition, dorsal and ventral EdU signals showed
157 similar distribution ranges in Mp*cps*^{ld} mutants, which was consistent with their flat morphology
158 under cW+cFR (Figure 1E).
159

160 **Mp*CPS* has a role in modulating gametangiophore development**

161 Continuous FR irradiation is known to induce sexual reproduction in *M. polymorpha*, i.e. the
162 formation of sexual branches called gametangiophores, and the differentiation of sexual
163 organs called gametangia (Yamaoka et al., 2018; Inoue et al., 2019). To observe this process,
164 plants were grown from gemmae under cW for 7 days, then transferred to cW+cFR for
165 gametangiophore induction. As a liverwort, *M. polymorpha* undergoes vegetative growth with
166 dichotomous branching, periodically multiplying the number of apical meristems through
167 bifurcation. Generally, all apical meristems remain indeterminate under white light conditions,
168 while a proportion of them become dormant or differentiate into gametangiophores under FR-
169 enriched light conditions (Streubel et al., 2023). During the induction under cW+cFR, we
170 observed higher numbers of total apical meristems in Mp*cps*^{ld} mutants than in wild-type or
171 complementation lines, which is in line with their more active vegetative growth (Figure 2A-B;
172 Supplemental Figure 4A). If the potential for apical meristems to form gametangiophores was
173 similar between the mutants and wild-type plants, higher number of gametangiophore-bearing
174 apexes would be expected in Mp*cps*^{ld} mutants. However, Mp*cps*^{ld} mutants formed fewer
175 gametangiophores than wild-type plants and complementation lines during the first 16 days
176 after FR irradiation, suggesting that gametangiophore formation is inhibited in these mutants
177 (Figure 2A-B; Supplemental Figure 4A).

178 In addition, the morphology of gametangiophores was distorted in Mp*cps*^{ld} mutants. As *M.*
179 *polymorpha* is a dioicous species, gametangiophores are sexually dimorphic among plants

180 with different sex chromosomes. The male gametangiophores (antheridiophores) of wild-type
181 plants had roundish, disc-like receptacles, which were ventrally connected to a relatively long
182 and thin stalk at the center. While for Mp*cps*^{ld} mutants, the male receptacles were fan-shaped,
183 attaching to a short and thick stalk(s) at the basal end (Fig 2C,E; Supplemental Figure 4B).
184 Transverse sectioning revealed thallus-like features in the stalks of Mp*cps*^{ld} antheridiophores.
185 Usually, no air chambers could be observed in the near-cylindric antheridiophore stalks of wild-
186 type plants. In contrast, Mp*cps*^{ld} antheridiophore stalks had a flat dorsal surface beneath which
187 air chambers with photosynthetic filaments were clearly formed (Supplemental Figure 5A),
188 quite similar to the tissue organization in the vegetative thallus (Shimamura, 2016). Besides,
189 Mp*cps*^{ld} antheridiophore stalks frequently have more canals with pegged rhizoids in the ventral
190 side, possibly reflecting additional bifurcation events during gametangiophore morphogenesis
191 (Supplemental Figure 5A).

192 The female gametangiophores (archegoniophores) of wild-type plants were also stalked and
193 had 9-11 finger-like structure (digitate rays) in the receptacle, which radially arranged like
194 umbrella ribs. Two marginal digitate rays could be recognized as no involucres were produced
195 between them (Figure 2D,F; Supplemental Figure 4B) (Cao et al., 2013). The female
196 receptacles of Mp*cps*^{ld} were palm-like, positioning the two marginal rays at opposite ends.
197 Excessive number of digitate rays and/or bifurcation in the stalk were often observed in late-
198 stage receptacles (Figure 2D,F; Supplemental Figure 4B). In extreme cases from aseptic
199 culture, the archegoniophore of Mp*cps*^{ld} remained the form of bifurcated thalloid branches, with
200 digitate rays formed at the thallus tips (Supplemental Figure 4C). If the relatively fixed number
201 of digitate rays in wild-type receptacles represents a determinate fate for the apical meristem,
202 such excessive bifurcation or additional digitate rays in Mp*cps*^{ld} mutants might suggest a loose
203 transition from the indeterminate vegetative growth. Similar to the male case, the stalks of
204 Mp*cps*^{ld} archegoniophores were shorter and thicker than the wild-type counterparts, bearing
205 more rhizoid canals in the ventral side (Figure 2D; Supplemental Figure 5C).

206 Since gametangium differentiation accompanies the morphogenesis of gametangiophores,
207 we investigated this progress by examining Citrine-labelled MpBONOBO proteins (MpBNB-Cit),
208 which specifically accumulate in the initial cells and immature gametangia (Yamaoka et al.,
209 2018). To keep the consistency in genetic background, large-deletions of Mp*CPS* were
210 introduced into Mp*BNB-Cit* knock-in lines through thallus transformation (Supplemental Figure

211 2), again using the CRISPR/Cas9^{D10A} nickase system (Hisanaga et al., 2019). As expected,
212 the gametangiophore morphogenesis was delayed by Mp*cps*^{ld} mutation. After 11 or 14 days of
213 growth under cW+cFR, dome-shaped gametangiophore primordia already formed, respectively,
214 in male and female Mp*BNB-Cit* plants carrying the wild-type Mp*CPS* allele. Under fluorescence
215 microscopes, arrays and/or clusters of Citrine signals appeared at the edge of primordia,
216 indicating on-going gametangium differentiation in these plants. In contrast, no
217 gametangiophore primordium was yet visible in Mp*cps*^{ld} Mp*BNB-Cit* lines of the same ages.
218 Few or no Citrine-positive nuclei could be found in the apical regions of these plants,
219 suggesting that Mp*cps*^{ld} also caused a delay in gametangium differentiation (Figure 2G-J).
220 Despite such delay, male and female gametangia of normal morphology eventually formed in
221 Mp*cps*^{ld} mutants, as shown by the longitudinal sections of the receptacles (Supplemental
222 Figure 5B,D). Crossing experiments further confirmed the fertility of gametes, as mature
223 spores could be produced from all combinations among Mp*cps*^{ld} and wild-type plants
224 (Supplemental Figure 5E-F).
225

226 **Mp*cps*^{ld} phenotypes can be rescued by *ent*-kaurenoic acid (KA)**

227 To explore the GA biosynthesis pathway possibly blocked by Mp*cps*^{ld}, we first investigated if
228 common GAs from angiosperms could be detected endogenously in *M. polymorpha*. The
229 plants were cultured for 10 days under cW, then 4 days under cW+cFR before harvested for
230 analysis with liquid chromatography-tandem mass spectrometry (LC-MS/MS). In the Tak-1
231 wild-type plants, GA_{12} but not any downstream compounds from the angiosperm GA
232 biosynthesis pathway could be detected (Figure 3A-B; Supplemental Figures 1 and 6A). The
233 endogenous level of GA_{12} is 28.9 ± 6.5 pg/g fresh weight on average, which is much lower
234 than the levels in the seedlings of *Arabidopsis thaliana* (Nomura et al., 2013). In Mp*cps-4*^{ld}
235 plants cultured under the same conditions, endogenous GA_{12} did not reach the detection limit,
236 which supported the loss of GA biosynthesis in this mutant (Figure 3B).

237 Next, we tested the effect of GA-related compounds on *M. polymorpha*. For thallus
238 morphology observation, gemmae were planted on agar medium containing different GAs or
239 the solvent control, then cultured under cW+cFR for 12 days. For gametangiophore induction,
240 plants were transferred onto agar medium containing chemicals at the onset of cW+cFR
241 induction. Several bioactive GAs in vascular plants and the GA biosynthesis precursor, KA,

242 were tested on wild-type and Mp*cps-4*^{ld} mutants. GA_{12} was not included in the assay due to its
243 limited availability. As a result, 2-μM KA application fully complemented Mp*cps-4*^{ld} phenotypes.
244 The thallus shape, the progress of gametangiophore formation and the gametangiophore
245 morphology were all restored to the manner of wild-type plants (Figure 3C-F). Furthermore, KA
246 treatment altered the thallus morphology of Mp*cps-4*^{ld} in a dose-dependent manner under
247 cW+cFR. 100-nM KA was sufficient to induce clear changes in the size, shape and hyponasty
248 of the mutant thallus (Supplemental Figure 7A, C-E). However, KA did not evidently change
249 the thallus shape or gametangiophore formation in wild-type plants, which suggested it to be a
250 biosynthetic intermediate rather than being directly bioactive. No active GAs in angiosperms
251 (GA_1, GA_3 or GA_4) rescued Mp*cps-4*^{ld} as efficiently as KA, which was consistent with their
252 absence in *M. polymorpha*. GA_9 methyl ester (GA_9-Me), which is released by several ferns as
253 a pheromone and could rescue Pp*cps/ks* phenotype in the moss *P. patens* (Yamauchi et al.,
254 1996; Tanaka et al., 2014; Hayashi et al., 2010), did not work on Mp*cps-4*^{ld} in *M. polymorpha*
255 (Figure 3C-F).
256 Taken together, these data indicated that Mp*cps*^{ld} phenotypes were likely caused by the
257 deficiency in some GA-related diterpenoid compound(s), which is synthesized from KA but
258 different from bioactive GAs in vascular plants. For convenience, hereafter we refer to this
259 putative bioactive compound as GA_{Mp}.
260

261 **MpKOL1 and MpKAOL1 catalyze the biosynthesis of KA and GA_{12}, respectively**

262 The enzymatic activities for MpCPS to produce *ent*-copalyl diphosphate and MpKS
263 (Mp6g05950) to produce *ent*-kaurene have been biochemically confirmed in the previous
264 research (Kumar et al., 2016). To find the downstream enzymes catalyzing KA and GA_{12}
265 biosynthesis in *M. polymorpha*, we tested the enzymatic activity of KO and KAO homologs
266 (Figure 4A). Three KO homologs were identified by phylogenetic analysis in *M. polymorpha*
267 (Supplemental Figure 8), and each of them was expressed in the methylotrophic yeast *Pichia*
268 *pastoris* together with the *Arabidopsis* CYTOCHROME P450 REDUCTASE 1 (AtCPR1,
269 AT4G24520). The yeasts were co-cultured with the substrate (*ent*-kaurene) for two days, then
270 the culture infiltrates were extracted and analyzed with gas chromatography-mass
271 spectrometry (GC-MS). KA was generated as a major product in the yeast culture expressing

272 MpKOL1 (Mp3g18320), but not detected in cultures expressing MpKOL2 (Mp2g01950) or
273 MpKOL3 (Mp2g01940) (Figure 4B; Supplemental Figure 6B).
274 All currently known plant-type KAOs belong to the CYP88 family, in which two *M.*
275 *polymorpha* members (MpKAOL1, Mp4g23680; and MpKAOL3, Mp2g10420) were confirmed
276 by our phylogenetic analysis. Previous analysis considered the protein encoded by
277 Mp1g25410 as a KAO homolog and named it MpKAOL2 (Bowman et al., 2017). In our current
278 analysis, this protein and its liverwort homologs were closely related to CYP729 family
279 members, which are distinctively different from CYP88 proteins (Supplemental Figures 9-10).
280 After two day's culturing, *Pichia* cells expressing MpKAOL1 showed a clear consumption of KA
281 and production of GA_{12}, which displayed identical retention time and mass spectra with the
282 major product from the AtKAO1-expressing culture, i.e. the positive control. While in the
283 MpKAOL3-expressing culture, consumption of KA was limited and no GA_{12} production was
284 detected (Figure 4C-D, Supplemental Figure 6B). It seems that MpKOL1 and MpKAOL1, but
285 not their *M. polymorpha* homologs, harbor catalytic activities similar to angiosperm GA
286 biosynthesis enzymes.
287 By expressing Citrine-fused proteins under the control of the 35S promoter, we observed the
288 subcellular localization of the four *M. polymorpha* enzymes which showed catalytic activities
289 related to GA biosynthesis (Supplemental Figure 11). MpCPS-Cit and MpKS-Cit proteins were
290 localized in the chloroplasts, most likely in the stroma as the Citrine signal intensities displayed
291 complementary patterns to the thylakoid-enriched chlorophyll (Supplemental Figure 11A-B).
292 The signals of MpKOL1-Cit proteins were also associated with chloroplasts, being strongest in
293 chloroplast envelopes (Supplemental Figure 11C). On the other hand, MpKAOL1-Cit proteins
294 seemed to aggregate in the endomembrane system and could be observed near the nuclear
295 envelope and the plasma membrane (Supplemental Figure 11D). Overall, the subcellular
296 distribution of these proteins were similar to their homologs in *A. thaliana* (Sun and Kamiya,
297 1994; Helliwell et al., 2001b), supporting them as being evolutionary conserved in land plants.
298

299 **KA is a pivotal intermediate in the biosynthesis of GA-related hormone**

300 To validate the physiological role of GA biosynthesis enzymes other than MpCPS *in vivo*, we
301 created loss-of-function mutants for all KS, KO and KAO homologs in *M. polymorpha*, using
302 the CRISPR/Cas9^{D10A} nickase or the CRISPR/Cas9 system (Supplemental Figure 2B-D;

303 Supplemental Figure 12). Consistent with the enzymatic activities in yeast or *in vitro* (Kumar et
304 al., 2016), Mp*ks-14*^{ld}, Mp*kol1-7*^{ld}, and Mp*kaol1-7*^{ge} mutants completely lost the ability to
305 produce GA_{12} endogenously (Figure 4E; Supplemental Figure 6C-D). Under cW+cFR
306 conditions, the phenotypes of Mp*ks*^{ld} and Mp*kol1*^{ld} mutants were similar to that of Mp*cps*^{ld}. The
307 thalli of these mutants were significantly larger, wider and flatter than those of wild-type plants
308 (Figure 4F-G). Mp*ks*^{ld} and Mp*kol1*^{ld} mutants were delayed in gametangiophore formation, and
309 their antheridiophores had fan-shaped receptacles and short thick stalks (Figure 4H-I). As
310 MpKS and MpKOL1 catalyze reactions prior to KA biosynthesis, we tested if KA could rescue
311 the phenotypes of Mp*ks*^{ld} and Mp*kol1*^{ld}. Indeed, 2-μM KA application fully restored the thallus
312 morphology and gametangiophore formation in these mutants, which further supported that KA
313 biosynthesis has a pivotal role in the FR response of *M. polymorpha* (Figure 4F-I).

314 In addition to MpKS, the other TPS-e/f clade member, MpTPS1 (Mp6g05430), is known to
315 produce *ent*-kaurene as a minor product (Kumar et al., 2016). However, Mp*tps1*^{ld} mutants
316 showed similar morphology to wild-type plants under cW or cW+cFR conditions, suggesting
317 that Mp*TPS1* is not a major gene required for GA_{Mp} biosynthesis (Supplemental Figure 12A;
318 Supplemental Figure 13). Mp*KOL2* and Mp*KOL3*, the homologs of Mp*KOL1*, are tandemly
319 arranged in the genome, so we removed the whole genomic fragment containing both genes
320 with CRISPR/Cas9^{D10A} nickase (Supplemental Figure 12B). Again, no phenotype related to FR
321 response was observed, which is consistent with the lack of KA-producing activity for both
322 enzymes (Supplemental Figure 13).

323 As MpKAOL1 could catalyze the KA to GA_{12} conversion, we hypothesized that this is a
324 reaction leading to the biosynthesis of GA_{Mp} in *M. polymorpha*. As a fact, Mp*kaol1*^{ge} mutants
325 were defective in FR response, in a manner similar to the KA biosynthesis mutants. After 12
326 days of growth under cW+cFR, large wide and flat thallus was observed in Mp*kaol1*^{ge} mutants
327 (Figure 4F-G). Since MpKAOL1 is likely to act downstream of KA synthesis, these mutants
328 were not supposed to be very sensitive to KA treatment. In the experiments, although 2 μM of
329 KA slightly altered the thallus morphology under cW+cFR, while no significant changes could
330 be observed at concentrations equal to or lower than 1 μM (Figure 4F-G; Supplemental Figure
331 7B-E). Mp*kaol1*^{ge} mutants also showed a moderate delay in gametangiophore formation, which
332 was insensitive to KA treatment. However, the antheridiophore morphology of Mp*kaol1*^{ge}
333 mutants was similar to that of wild-type plants, suggesting that the biosynthesis of GA_{Mp} might

not be completely abolished by Mp*kaol1*^{ge} (Figure 4H-I). Complete deletion of the other KAO homolog, Mp*kaol3*^{ld}, failed to show any severe defects in FR response, yet double mutants would be needed for future research to carefully examine the redundancy with MpKAOL1 (Supplemental Figures 12C and 13).

FR enrichment induced GA biosynthesis in a Mp*PIF*-dependent manner

Recent research reported that several GA biosynthesis genes were up-regulated under FR-enriched light conditions (Briginshaw et al., 2022). In our previous transcriptome data (Hernández-García et al., 2021), irradiation solely with FR light significantly increased the expression of Mp*KOL1* within 1 h, and the expression of Mp*CPS* and Mp*KAOL1* after 4 h of treatment. Such responses were only seen in the wild-type plants but not the Mp*pif*^{ko} mutant, indicating that it is a process controlled by the Mpphy-MpPIF signaling module (Supplemental Figure 14A). Similarly, when we transferred 7-day-old plants grown under cW conditions to cW+cFR, Mp*PIF*-dependent up-regulation of Mp*CPS*, Mp*KS*, Mp*KOL1* and Mp*KAOL1* expression could be detected by quantitative polymerase chain reaction (qPCR) within 24 h (Figure 5A, Supplemental Figure 14B). Interestingly, Mp*KOL1* showed a slightly different expression pattern to the other three genes. MpKOL1 expression peaked at 8 h after induction but slightly decreased at the 24-h time point, while the expression of Mp*CPS*, Mp*KS* and Mp*KAOL1* gradually increased in the 24 h after induction, which might reflect different modes of transcriptional regulation. Consistent with the gene expression, we detected a higher level of endogenous GA_{12} in plants induced with cW+cFR than those kept under cW conditions, which suggested the accumulation of GA-related compounds under FR-enriched conditions (Figure 5B).

GA-related hormone regulated transcriptional responses to FR enrichment

To explore gene expression changes related to GA biosynthesis in *M. polymorpha*, we analyzed transcriptomes from thalli grown under cW or cW+cFR for 12 days, either of wild-type plants, or of Mp*cps-4*^{ld} mutants with or without 2-μM KA treatment. In agreement with the mild change in thallus morphology, only a few genes were differentially expressed between Mp*cps-4*^{ld} and wild-type plants under cW conditions (Figure 5C; Supplemental Data Set 1). In particular, the expression of Mp*TPS6*, which encodes an enzyme producing *cis*-kolavenol (Jia

365 et al., 2022), was significantly decreased in Mp*cps-4*^{ld} and rescued by KA under cW. In
366 contrast, 780 and 257 genes were down- and up-regulated, respectively, in Mp*cps-4*^{ld} mutants
367 under cW+cFR, suggesting a more active function of GA_{Mp} under FR-enriched conditions. A
368 proportion of the differentially expressed genes could be rescued by KA application (Figure 5C;
369 Supplemental Data Set 1). For most of the Mp*cps*^{ld}-affected genes, the expression was
370 strongly altered by FR enrichment in the wild-type plant, and the differential expression in
371 Mp*cps-4*^{ld} was essentially the reduction in FR-induced gene expression change (Figure 5D). If
372 we compare the transcriptomes between cW+cFR and cW, the numbers of up- and down-
373 regulated genes both declined by more than 60% in the Mp*cps-4*^{ld} mutant (Figure 5E).
374 Using fussy gene ontology (GO) annotations generated with the Blast2GO algorithm
375 (Conesa and Götz, 2008; Hernández-García et al., 2021), we performed GO enrichment
376 analyses for biological processes on differentially expressed genes in Mp*cps-4*^{ld} under
377 cW+cFR (Figure 5F; Supplemental Data Set 2). Although KA application rescued only a limited
378 proportion of gene expression changes in Mp*cps*^{ld}, the patterns of enriched GO terms were
379 quite similar in both comparisons. Mp*cps-4*^{ld} down-regulated or KA-upregulated genes were
380 enriched in GO terms related to stress response and secondary metabolism, among which top-
381 ranked the phenylpropanoid metabolic process. When we carefully checked gene homologs,
382 23 genes putatively catalyzing biosynthesis of auronidins, bibenzyls or lignin monomers were
383 up-regulated by FR enrichment in a Mp*CPS*-dependent manner (Supplemental Figure 15A). In
384 the Mp*cps-4*^{ld} down-regulated gene set, we also found 30 CYPs, 12 2-OGDs and 7 uridine 5'-
385 diphospho-glucuronosyltransferases (UGTs), all of which were mostly homologs specific to *M.*
386 *polymorpha* or liverworts, possibly associated with lineage-specific metabolites (Supplemental
387 Figure 15B-D). It seemed that *M. polymorpha* was allocating more resources to stress and
388 defense responses under FR-enriched conditions, yet less doing so when GA_{Mp} biosynthesis
389 was defective. On the other side, GO enrichment captured photosynthetic genes in the Mp*cps-*
390 *4*^{ld} up-regulated gene set (Figure 5F), which suggested that this mutant might be more
391 resistant to FR-induced chlorophyll reduction (Fredericq and de Greef, 1966). Cell-wall related
392 enzymes and peroxidases were found in both down- and up-regulated gene sets, which was in
393 agreement with the change in thallus growth allometry caused by FR enrichment or Mp*cps*^{ld},
394 but might also be related to stress and defense responses (Supplemental Figure 15E-F).

395 Gene expressions of several phytohormone pathways were altered by Mp*cps*^{ld} under
396 cW+cFR. First of all, FR-induction of Mp*KS* and Mp*KAOL1* was reduced in Mp*cps-4*^{ld}, which
397 suggested that GA biosynthesis might be regulated by positive feedback in *M. polymorpha*
398 (Supplemental Figure 15G). Such an effect was confirmed with qPCR, in which 3 days of KA
399 treatment partially restored Mp*KS* and Mp*KAOL1* expression (Figure 5G). Mp*KOL1* expression
400 was not affected by Mp*cps*^{ld} or KA treatment, suggesting that it is not a target for such
401 feedback regulation. For cytokinin, the biosynthesis enzymes Mp*IPT2* and Mp*LOG*, and the
402 deactivation enzyme Mp*CKX2* were down-regulated in Mp*cps-4*^{ld} (Supplemental Figure 15G).
403 Previous research showed that Mp*CKX2* overexpression reduced the level of cytokinins,
404 restricted thallus growth and increased thallus hyponasty under cW (Aki et al., 2019). It is
405 possible that FR enrichment changed the thallus growth via coordinated deactivation of
406 cytokinins and accumulation of GA_{Mp}. Furthermore, expression of three abscisic acid (ABA)
407 metabolic genes (MpABA4, MpNCED, MpCYP707A) and more than 40 ABA-responsive, LATE
408 EMBRYOGENESIS ABUNDANT-like (LEA-like) proteins were induced by FR enrichment,
409 similar to the response in *A. thaliana* (Michaud et al., 2023) (Supplemental Figure 15H). Such
410 induction was reduced in Mp*cps-4*^{ld} and restored by KA application, which showed similar
411 tendency as the overall stress response.
412

413 **DISCUSSION**

414 Light quality, i.e. the ratio of red and far-red lights, is an important environmental clue for
415 nearly all land plants to optimize their growth and photosynthesis efficiency. Using a reverse-
416 genetic approach, we showed that biosynthesis of gibberellin-related diterpenoids is required
417 for many aspects of FR response in the liverwort *M. polymorpha*. Under FR-enriched
418 conditions, wild-type plants often develop narrow and hyponastic thallus and begin to form
419 gametangiophores, which is accompanied with increased expression of GA biosynthesis
420 genes and accumulation of GA_{12} (Figures 1, 2, 5) (Fredericq and de Greef, 1966; Briginshaw
421 et al., 2022). In contrast, Mp*cps*^{ld} and other GA biosynthesis mutants developed wide and flat
422 thallus, with a delay in the gametangiophore formation (Figures 1, 2, 4). Application of the
423 biosynthesis intermediate KA rescued all mutants deficient of its biosynthesis (Figures 3, 4),
424 indicating that these phenotypes were likely caused by the deficiency of some KA-derived
425 diterpenoid compound(s), which we named GA_{Mp}. In angiosperms, GA constantly modulates

426 growth and development throughout the life cycle, mostly by promoting growth via cell
427 elongation and/or cell division (Hedden, 2020). But in *M. polymorpha*, GA_{Mp} deficiency had little
428 influence on the vegetative growth under white light conditions. The bioactivity of GA_{Mp} was
429 observed only after its induced accumulation under FR-enriched conditions, suggesting that it
430 served as a hormone coping with environmental changes, rather than constitutively regulating
431 growth. Moreover, the thallus size was increased in GA_{Mp} biosynthesis mutants under cW+cFR
432 (Figures 1, 4), implying that GA_{Mp} actively inhibits rather than promotes growth in the
433 gametophyte of *M. polymorpha*.

434 FR enrichment induced hyponastic growth in the thallus of *M. polymorpha*, which is
435 comparable to the increase of leaf hyponasty in shade-avoiding angiosperms. In *A. thaliana*,
436 FR enrichment triggers the hyponastic growth by preferentially enhancing cell elongation in the
437 abaxial side of the petiole (Küpers et al., 2023). While in *M. polymorpha*, such response relies
438 on the regional growth driven by apical meristems. In previously reported end-of-day FR
439 irradiation experiments, if the treatment was discontinued after several cycles, the newly-grown
440 apical region resumed pleiotropic orientation, while the basal part remained hyponastic
441 (Fredericq and Greef, 1968). With EdU analysis, we observed cell division patterns under FR-
442 enriched conditions, which was most active near the apical meristem. The hyponastic growth
443 in wild-type plants were marked with excessive cell division in the ventral side of the thallus,
444 implying a role for differential cell proliferation in this process. The large and flat thallus of
445 Mp*cps*^{ld} mutants have more actively dividing cells in total, which showed no dorsiventrally
446 biased distribution (Figure 1). Since Mp*cps*^{ld} phenotypes could be complemented by
447 expression of Mp*CPS* using the constitutive 35S promoter, which was equally active in dorsal
448 and ventral tissues (Althoff et al., 2014), it is unlikely that FR-induced hyponasty is established
449 directly by differential biosynthesis of GA_{Mp}. This is similar to the situation in *A. thaliana*
450 petioles, where GA served as a modulator for FR-induced hyponasty but showed no biased
451 adaxial-abaxial activity (Küpers et al., 2023).

452 The erected, stalked gametangiophores of *M. polymorpha* could be considered as an
453 extreme form of hyponastic growth, and dorsal tissues were evidently reduced in the cylindrical
454 stalks of wild-type plants (Shimamura, 2016). The stalks of Mp*cps*^{ld} gametangiophores were
455 relatively short and thick, bearing dorsal air chambers similar to the vegetative thallus, which
456 showed less biased dorsoventral growth (Figure 2; Supplemental Figure 5). This phenotype

457 resembled that of Mp*kanadi* (Mp*kan*), which was depleted of the sole *M. polymorpha* homolog
458 for KANADI, a family of transcription factors regulating tissue polarity in angiosperms
459 (Briginshaw et al., 2022). Under cW+cFR, both Mp*kan* and Mp*cps*^{ld} mutants were reduced in
460 hyponasty, formed thallus-like gametangiophores with delay but generated fertile gametes,
461 which could be explained by the dysfunction of Mp*kan* to up-regulate the expression of GA_{Mp}
462 biosynthesis genes in response to FR irradiation (Briginshaw et al., 2022).

463 By tracing germ cell progenitors with MpBNB accumulation, we found that Mp*cps*^{ld} mutants
464 were delayed in germline differentiation (Figure 2). Many fern species use GA-related
465 pheromones, i.e. antheridiogens, to control germline differentiation in the population.
466 Particularly, antheridiogens promote the formation of male antheridia, and inhibits female
467 archegonia in undifferentiated gametophytes (Näf et al., 1975; Tanaka et al., 2014; Hornych et
468 al., 2021). In *M. polymorpha*, sexual differentiation is known to be determined by a sex
469 chromosome-located gene (Iwasaki et al., 2021), and MpBNB accumulation was similarly
470 delayed in both male and female Mp*cps*^{ld} gametophytes, suggesting no sexual bias in the
471 function of GA_{Mp}.

472 We partially elucidated the biosynthetic pathway of GA_{Mp} with biochemical and genetic
473 approaches. Previous bioinformatic research suggested that early steps of GA biosynthesis
474 are conserved in land plants, and the *M. polymorpha* genome contains multiple homologs for
475 KO and KAO (Bowman et al., 2017; Cannell et al., 2020; Yoshida et al., 2020). Using the yeast
476 expression system, we detected the production of KA by MpKOL1 and GA_{12} by MpKAOL1,
477 showing the two enzymes possessing enzymatic activities similar to their angiosperm
478 homologs. Genetic analyses also supported that KA is synthesized via the sequential action of
479 three single enzymes (Mp*CPS*, Mp*KS*, and Mp*KOL1*), as their mutants were consistently
480 defective in FR light responses (Figure 4). Intriguingly, although GA_{12} production was almost
481 completely blocked in Mp*kaol1*^{ge} mutants, we only saw morphological phenotypes in the
482 vegetative thallus, but not in the gametangiophores. As monooxygenases, it takes three
483 sequential steps for CYP enzymes to catalyze the KA-to-GA_{12} conversion, first from KA to *ent*-
484 7-hydroxy-kaurenoic acid (7OH-KA), then from 7OH-KA to GA_{12}-aldehyde, and finally from
485 GA_{12}-aldehyde to GA_{12} (Helliwell et al., 2001a). In the GA-producing fungus *Fusarium fujikuroi*,
486 even though GA_{12} production still occurs, it is largely bypassed through 3β-hydroxylation of
487 GA_{12}-aldehyde to form GA_{14}-aldehyde, which is then converted into GA_{14} and other gibberellin

488 compounds (Hedden et al., 1974; Urrutia et al., 2001; Rojas et al., 2001). Therefore, we could
489 not conclude that Mp*kaol1*^{ge} mutant phenotypes were caused by deficiency in GA_{12} production,
490 and MpKAOL1 might work redundantly with other enzymes to produce other intermediates,
491 synthesizing GA_{Mp} in a GA_{12}-independent pathway.

492 Despite the conserved activities of MpKOL1 and MpKAOL1, we detected no KA synthesis
493 activity for MpKOL2 or MpKOL3, and no GA_{12} production by MpKAOL3 (Figure 4). Also, no
494 morphological abnormality related to far-red light response was observed in their loss-of-
495 function mutants, suggesting that they are not major enzymes required for GA_{Mp} biosynthesis
496 (Supplemental Figure 13). In the phylogenetic tree of KOs (CYP701s) (Supplemental Figure 8),
497 all liverwort homologs formed a monophyletic clade with two major subclades, both containing
498 sequences from Jungermanniopsida and Marchantiopsida species. MpKOL2 and MpKOL3
499 belong to a subclade different from MpKOL1, suggesting these KO homologs were diverged
500 soon after the emergence of the most recent liverwort common ancestor. The phylogenetic
501 relationship of KAOs (CYP88s) from liverworts and hornworts is less clear, but similarly,
502 MpKAOL1 and MpKAOL3 belong to different clades deeply diverged in liverworts
503 (Supplemental Figure 9). It remains to be explored if such divergence contributes to the
504 diversification of diterpenoid metabolism in liverworts.

505 Comparing the biosynthesis of GA-related diterpenoids between *M. polymorpha* and *P.*
506 *patens*, we see both conservation and divergence of this pathway in evolution. On the one
507 hand, both bryophyte species share the biosynthesis route for KA with vascular plants. KO is
508 present in almost all genomes and transcriptomes included in our phylogenetic analysis. As a
509 recent study proposed that the ancestral *TPS* gene in land plants encoded a bifunctional
510 CPS/KS enzyme (Jia et al., 2022), it is possible that production of KA is conserved in all major
511 lineages of land plants. On the other hand, *M. polymorpha* and *P. patens* seem to take
512 different routes to synthesize bioactive compounds from KA. Consistent with the lack of KAO
513 (CYP88) homologs in all mosses, *P. patens* produced *ent*-3β-hydroxy-kaurenoic acid (3OH-KA)
514 and *ent*-2α-hydroxy-kaurenoic acid (2OH-KA) from KA, with the former having physiological
515 activities on protonemal cell differentiation (Miyazaki et al., 2018). Meanwhile, the production of
516 GA_{12} in *M. polymorpha* opened the possibility of using C20-GAs in growth regulation, although
517 no common GA from angiosperms was detected in either bryophyte species (Figure 3)
518 (Hayashi et al., 2010).

Due to the lack of GIBBERELLIN-INSENSITIVE DWARF1 (GID1) receptors in bryophytes, it is unlikely that GA-related hormones are perceived by the canonical GID1-DELLA module in *M. polymorpha* or *P. patens*. Previously we reported that overexpression of Mp*DELLA* inhibited MpPIF-mediated FR responses, reducing gemma dormancy and delaying the formation of gametangiophores (Hernández-García et al., 2021). However, Mp*DELLA* overexpression strongly inhibited cell division and thallus growth, which was opposite to the effect of GA_{Mp} deficiency. It is possible that the functions of GA_{Mp} and MpDELLA remain uncoupled in *M. polymorpha*.

Gene expression analysis confirmed that Mp*CPS*, Mp*KS*, Mp*KOL1* and Mp*KAOL1* were induced by FR enrichment in an Mp*PIF*-dependent manner (Figure 5). The regulatory role of Mp*PIF* is further supported by phenotypic similarities between GA_{Mp} biosynthesis mutants and Mp*pif*. Under FR enriched conditions, Mp*pif* mutants developed wider, flatter and larger thallus, and failed to form any gametangiophores (Inoue et al., 2019; Streubel et al., 2023). In angiosperms, FR enrichment also activates the expression GA biosynthesis enzymes, yet more frequently regulating 2-OGD family genes such as GA20ox or GA3ox (Hisamatsu et al., 2005; Kohnen et al., 2016; Küpers et al., 2023), which are absent from bryophytes. Considering the putatively different mechanism for GA perception, GA biosynthesis might be independently incorporated into the gene regulatory network by liverworts and angiosperms in evolution, in response to the common threat of a FR-enriched environment.

METHODS

Plant materials and maintenance

The *M. polymorpha* subsp. *ruderalis* accessions Takaragaike-1 (Tak-1) and Takaragaike-2 (Tak-2) were used as male and female wild-type materials, respectively (Ishizaki et al., 2008). For maintenance, *M. polymorpha* plants were cultured aseptically on half-strength Gamborg's B5 medium (Gamborg et al., 1968) with 1% agar at 22°C under continuous white light (40-50 µmol photons m^{-2} s^{-1}), which was supplemented by cold cathode fluorescent lamps (CCFLs, OPT-40C-N-L from Optrom, Japan). If not specified, this medium and temperature was used for all aseptic cultures for *M. polymorpha*.

549 **Light sources**

550 In all the experiments, plants were cultured under continuous white light conditions (cW,
551 approximately 40 μmol photons m^{-2} s^{-1}) with or without continuous far-red light (cFR,
552 approximately 25 μmol photons m^{-2} s^{-1}). For thallus morphology observation, cW and cFR were
553 supplemented by CCFLs and light-emitting diodes (LEDs), respectively, in the multi-
554 chambered incubator (LH-80CCFL-6CT from NK systems, Japan). For gametangiophore
555 induction of aseptic cultures, cW was supplemented by CCFLs (ST-40C-BN, Shinshu Trading,
556 Japan) and cFR was supplemented by LEDs (IR LED STICK, NAMOTO, Japan). For plants
557 grown on the vermiculite, cW was supplemented by fluorescent tubes (FLR40SN/M/36,
558 Toshiba, Japan) and cFR was supplemented by LEDs (VBL-TFL600-IR730, Valore, Japan).

559

560 **Construction of mutants and transgenic plants**

561 To create large-deletion mutants of a target gene, four guide RNAs (gRNAs) with target
562 sequences flanking the CDS were first cloned separately into pMpGE_En04, pBCGE12,
563 pBCGE23 and pBCGE34 (Hisanaga et al., 2019; Koide et al., 2020) by ligation of BsaI-
564 digested vectors with annealed complementary DNA oligos. Then the fragments containing the
565 MpU6-1 promoter and gRNAs were digested from the pBCGE12, pBCGE23 and pBCGE34
566 constructs and inserted between the BglI sites of the pMpGE_En04 construct to create a
567 multiplex entry vector. Finally, this entry vector was recombined with pMpGE017 or pMpGE018
568 (Hisanaga et al., 2019) using Gateway LR Clonase II (Thermo Fisher Scientific) to generate
569 the binary vector for plant transformation. To generate the Mp*kaol1*^{ge} mutants, the gRNA was
570 designed to target sequences near the start codon of Mp*KAOL1*. The corresponding DNA
571 oligos were annealed and ligated into the BsaI sites of pMpGE_En03, then subcloned to the
572 binary vector pMpGE011 (Sugano et al., 2018).

573 For the complementation of mutants and/or subcellular localization observations, CDSs of
574 Mp*CPS*, Mp*KS*, Mp*KOL1* and Mp*KAOL1* were amplified from the complementary DNA (cDNA)
575 of Tak-1 plants and directionally cloned into pENTR/D-TOPO (Thermo Fisher Scientific) to
576 create entry vectors without stop codon. To mutate the gRNA target sequence in Mp*KAOL1*,
577 the whole plasmid of pENTR-MpKAOL1-CDS was amplified with the site-directed mutagenesis
578 primers MpKAOL1-mut-F and MpKAOL1-mut-R, then re-circularized to generate pENTR-
579 MpKAOL1-CDSmut. All the CDSs were then subcloned from entry vectors to pMpGWB106 or

580 pMpGWB306 using Gateway LR reactions, which were used for expressing the target proteins
581 under the 35S promoter with an in-frame Citrine fusion at the C terminus (Ishizaki et al., 2015).
582 All the binary vectors were introduced into *M. polymorpha* by transformation of regenerating
583 thalli using the *Agrobacterium tumefaciens* strain GV2260 as previously described (Kubota et
584 al., 2013). Successful mutations were identified by genotyping PCR and Sanger-sequenced to
585 confirm non-identical alleles. See Supplemental Tables 1-3 for full lists of plant materials
586 generated by this research, and the plasmids and DNA oligos used for construction.
587

588 **Measurement of thallus morphology**

589 For thallus morphological observation, plants were grown from gemmae on the medium
590 containing 1% sucrose under cW or cW+cFR in a multi-chambered incubator (LH-80CCFL-
591 6CT from NK systems, Japan). After 12 days of growth, camera photos of the plants were
592 taken vertically from the top. Then medium blocks with individual plants were carefully cut out,
593 aligned at a certain distance to a fixed camera for taking side-view photos. Typically, the two
594 apical meristems from one gemma both develop into mature thallus branches, and we define
595 the part developed from a single gemma meristem as a “half thallus”. These half thalli were cut
596 apart, flattened on a filter paper and photographed for the measurements of length, width and
597 area. All the measurements were done in Fiji (Schindelin et al., 2012) as describe in
598 Supplemental Figure 16 with in-house macro scripts, which are available at
599 https://github.com/dorrenasun/Mp_GA_biosynthesis. Data was excluded for a whole plant if
600 more than two apical meristems were active in the gemma, or for a half thallus if it showed
601 severe defects in dorsoventral differentiation.
602

603 **EdU assay**

604 To analyze the cell division activity, plants were grown on the medium containing 1%
605 sucrose under cW+cFR for 7 days, then soaked for 2 h in liquid half-strength Gamborg’s B5
606 medium containing 20 mM 5-ethynyl-2'-deoxyuridine (EdU). Then the samples were fixed in
607 3.7% formaldehyde for 1 h, washed twice with phosphate buffer saline (PBS, 5 min each), and
608 treated with 0.5% Triton X-100 in PBS for 20 min. After two washes with 3% bovine serum
609 albumin (BSA) in PBS, the samples were kept in the reaction mixture from the Click-iT EdU
610 Imaging Kit with Alexa Fluor 555 (Thermo Fisher Scientific, #C10338) for 1 h in darkness, then

611 washed twice with PBS before soaked overnight in 20% caprylyl sulfobetaine (#D4246, TCI,
612 Japan) to remove the chlorophyll. After another two washes with PBS, the thalli were treated
613 with 75.5% (w/v) iohexol (GE Healthcare Pharma) for 1 h and mounted on glass slides
614 following the iTOMEI protocol (Sakamoto et al., 2022). Image stacks of the apical regions were
615 obtained with a confocal laser scanning microscope (Olympus FLUOVIEW FV1000) at 5-μm
616 steps in the z direction. Excitation and emission wavelengths were 543 nm and 505-605 nm,
617 respectively. Numbers of EdU-positive nuclei were quantified in the Z-projections of the image
618 stacks using the StarDist plugin of Fiji and in-house scripts (Schmidt et al., 2018; Schindelin et
619 al., 2012).
620

621 **Observation of gametangiophores**

622 To observe the progress of gametangiophore formation in aseptic culture, plants were first
623 grown from gemmae on the medium containing 1% sucrose under cW for 7 days, then half
624 thalli developed from single gemma meristems were cut apart and cultured on fresh medium
625 plates under cW+cFR. Chemical treatments were included in the medium of second-stage
626 culturing, starting together with the FR irradiation. Apical regions of each plant were observed
627 under a stereoscope (Olympus SZX16) every day, and the emergence of gametangiophores
628 was recorded if a stalk or dark-green primordia was formed. Images of gametangiophores
629 were taken with stereoscopes (Olympus SZX16 or Leica M205C). For morphological
630 observation of gametangiophores, the plants were also grown on the vermiculite in the open
631 air. After an initial culturing of 7-14 days from gemmae under aseptic maintenance conditions,
632 thallus fragments were planted in pots containing vermiculite and grown under cW+cFR
633 conditions with regular watering. For sectioning of gametangiophores, fresh stalks or
634 receptacles were embedded in 5-6% agar and sectioned with a vibratome (DOSAKA
635 LinearSlicer Pro7) at the desired thickness. Images of the sections were obtained with the
636 microscope under bright field (Keyence BZ-X710).
637

638 **Microscopy of MpBNB-Cit**

639 To capture the early stage of gametangium differentiation, male and female plants carrying
640 the Mp*BNB-Cit* knock-in locus were cultured from gemmae on the medium containing 1%
641 sucrose under cW+cFR for 11 and 14 days, respectively. For male plants, half thalli developed

642 from single gemma meristems were collected for observation. For female plants, the second
643 bifurcation has already occurred, so one of the four apical regions was selected randomly on
644 each plant for observation. Thallus fragments were fixed with 4% paraformaldehyde (PFA) for
645 1 h at room temperature, washed twice with PBS and soaked in the ClearSeeAlpha solution
646 (Kurihara et al., 2021) for 2 days to remove chlorophyll. After that, the samples were washed
647 twice with PBS, stained with 1 mg/mL calcofluor white for 10 min and washed again twice with
648 PBS. Finally, the samples were infiltrated with 75.5% (w/v) iohexol (GE Healthcare Pharma) for
649 1 h and mounted onto slides. Image stacks were obtained with the fluorescent microscope
650 (Keyence BZ-X710) at 5-μm steps and processed into full-focus projections with BZ-X
651 Analyzer, and the number of Citrine-positive nuclei was counted in Fiji (Schindelin et al., 2012).
652 The BZ-X DAPI (Excitation: 360±20 nm; Emission: 460±25 nm; Dichroic mirror: 400 nm) and
653 customized (Excitation: 500±10 nm; Emission: 535±15 nm; Dichroic mirror: 515 nm) filters
654 were used for acquiring signals from calcofluor white and Citrine, respectively.
655

656 **LC-MS/MS analysis of endogenous GAs**

657 To analyze the endogenous GAs, most plants were cultured from gemmae on the medium
658 containing 1% sucrose under cW for 10 days, then under cW+cFR for another 4 days. Tak-1
659 wild-type plants were also cultured under cW for 14 days to examine the effect of FR
660 enrichment. For each sample, 3 g of thallus tissue was harvested, frozen with liquid nitrogen,
661 and stored at -80 °C before extraction. To prepare samples for LC-MS/MS analysis, each
662 frozen sample was homogenized in 15 mL acetone with $^{2}H_{2}$-labelled authentic compounds,
663 then left at 4 °C for a 2-h extraction. After filtering with defatted cotton, the acetone extract was
664 concentrated to approximately 1 mL with nitrogen blow and mixed with 1 mL acetonitrile. The
665 mixture was extracted for 3 times with 2 mL hexane, and the remaining aqueous phase was
666 alkalified with 1 mL saturated solution of $NaHCO_3$. After two more extractions with 2 mL
667 chloroform, the aqueous phase was passed through a cartridge filled with polyvinylpyrrolidone
668 (PVP), acidified to pH2-3 with HCl (6 M), and sequentially purified with a reverse-phase
669 cartridge (Oasis HLB 3 cc/60 mg, Waters), an anion-exchange cartridge (Bond Elut DEA 100
670 mg/1 mL, Agilent), and a silica cartridge (Sep-Pak Silica 1 cc Vac Cartridge, Waters). The final
671 elute was dried up with a vacuum centrifuge concentrator and dissolved in 1% acetic acid
672 before loading to the LC-MS/MS.

673 The LC-MS/MS system consisted of an ultra-performance LC (ExionLC, Sciex) equipped
674 with a reverse-phase column (CORTECS UPLC C18+, φ1.6 μm, 2.1×100 mm, Waters) and a
675 quadrupole time-of-flight mass spectrometer (X500R QTOF, Sciex). LC separations were
676 performed at 40 °C with a flow rate of 0.3 mL/min using solvent A (0.05% acetic acid in water)
677 and solvent B (0.05% acetic acid in acetonitrile) and the following program: a linear gradient of
678 B from 3% to 65% over 17 min, followed by an isocratic elution with 98% of B for 2 min.
679 Quantification of GAs was performed in the multiple reaction monitoring (MRM) mode, and the
680 mass spectrum of GA_{12} was confirmed in the TOF-MS/MS mode.
681

682 **Phylogenetic analysis**

683 For the phylogenetic analysis of KO and KAO homologs, the known protein sequences from
684 *A. thaliana* and *Oryza sativa* were used as the input for BLAST (Altschul et al., 1990) search in
685 the annotated proteins from published genomes and transcriptomes (See Supplemental Data
686 Set 3 for a full list of species and references). Considering the relative low redundancy of these
687 enzymes, the top 20 BLAST hits from each species were retrieved and aligned with MAFFT
688 using the progressive FFT-NS-2 algorithm (Katoh and Standley, 2013). After removing the
689 positions with >80% gaps, an initial maximum likelihood phylogenetic tree was built with all
690 candidate sequences using IQ-TREE 2 with automatic substitution model selection
691 (ModelFinder) and 1000 bootstraps from the ultrafast bootstrap approximation (UFBoot) (Minh
692 et al., 2020; Kalyaanamoorthy et al., 2017; Hoang et al., 2018). Highly-relevant candidate
693 sequences and outgroup sequences were selected from the initial tree and re-aligned with
694 MAFFT using the L-INS-I algorithm (Katoh and Standley, 2013) and trimmed off positions
695 with >98% gaps. The final maximum likelihood tree was inferred using IQ-TREE 2 with
696 automatic substitution model selection (LG+I+G4 for both KOs and KAOs) and 1000 standard
697 non-parametric bootstraps (Minh et al., 2020; Kalyaanamoorthy et al., 2017; Hoang et al., 2018;
698 Guindon et al., 2010). The complete pipeline including scripts, sequence alignments, and the
699 data file for the phylogenetic trees are available at
700 https://github.com/dorrenasun/Mp_GA_biosynthesis. The ggtree R package suite was used for
701 visualization (Yu, 2022; Xu et al., 2022; Yu, 2020b; Yu et al., 2018, 2017).
702

703 **Enzymatic assay in *P. pastoris* and GC-MS analysis**

704 To express MpKOLs and MpKAOLs in the yeast *P. pastoris*, the CDSs were amplified from
705 pENTR-CDS entry vectors and inserted into the pPICZA vector (Thermo Fisher Scientific) with
706 homologous recombination using the seamless ligation cloning extract (SLiCE) from
707 *Escherichia coli* (Zhang et al., 2012; Motohashi, 2015). The CDSs of At*KO* (AT5G25900) and
708 At*KAO1* (AT1G05160) were amplified from the cDNA of 14-day-old Col-0 seedlings and cloned
709 into pPICZA with the same method. All these plasmids were transformed into a previously
710 described *P. pastoris* X-33 strain carrying the *A. thaliana* cytochrome reductase gene, At*ATR1*
711 (AT4G24520) (Katsumata et al., 2008), following the manufacturer's protocol. The selected
712 transformants were incubated in 2 mL of BMG medium (100 mM potassium phosphate (pH
713 6.0), 1.34% yeast nitrogen base (YNB), 4×10^{-5}% biotin, 1% glycerol) with shaking at 30 °C until
714 they reached an OD_{600} value of 2. Cells were collected by centrifugation and resuspended in
715 50 mL of MM medium (1.34% YNB, 4×10^{-5}% biotin, 0.5% methanol), and cultured at 30 °C with
716 shaking and addition of methanol every 24 h (final concentration: 0.5% v/v) to maintain protein
717 induction. After 24 h of initial culturing, substrates (7 μg of *ent*-kaurene, or 15 μg of KA) were
718 added into the medium. After another 48 h of incubation, the supernatants were isolated with
719 centrifugation and extracted two times with equal volume of ethyl acetate. The organic phase
720 from the two extractions were combined together, concentrated *in vacuo*, and derivatized with
721 diazomethane in ether solution. After that, the samples were concentrated to approximately
722 100 μL with nitrogen blow and subjected to GC-MS analysis with a GC (Agilent 6890)
723 equipped with a DB-1 capillary column (15 m/0.25 mm/0.25 μm, Agilent J&W) and a mass
724 selective detector (Agilent 5975C MSD, ionization energy at 70 eV). The oven temperature
725 was programmed as described previously (Hayashi et al., 2006).

726

727 **Subcellular localization of proteins**

728 To observe the subcellular localizations of MpCPS, MpKOL1 and MpKAOL1, plants were
729 grown from gemmae on the medium containing 1% sucrose under cW+cFR conditions for 7
730 days. The thallus tissues were fixed with 4% PFA at room temperature for 20 min, washed
731 twice with PBS, and stained with 1 mg/mL calcofluor white for 10 min. After another two
732 washes with PBS, the samples were soaked in 75.5% (w/v) iohexol (GE Healthcare Pharma)
733 for 1 h and mounted onto slides. For MpKS, fresh gemmae from gemma cups were mounted in

734 water. For all experiments, complementation lines which used the 35S promoter to express
735 target proteins fused with Citrine in the C-teminus were used for observation, and the parent
736 lines of genetic mutants were used as the negative control.

737 Fluorescent images were acquired using a confocal microscope (Leica TCS SP8X Falcon)
738 equipped with a hybrid detector (HyD). For the observation of MpCPS-Cit and MpKS-Cit,
739 calcofluor white signals were excited with the 405 nm UV laser, and obtained in the xyz mode
740 within the 425-435 nm wavelength region; the Citrine signals were excited with the the pulsed
741 white light laser (WLL) at 488 nm, and obtained at 500-541 nm with time gating (1.8-12 ns for
742 MpCPS-Cit; 1.2-12 ns for MpKS-Cit); the autofluorescence from chlorophyll was excited with
743 the WLL at 592 nm, and obtained at 680-700 nm. For the observation of MpKOL1-Cit and
744 MpKAOL1-Cit, calcofluor white signals were excited with the 405 nm UV laser, and obtained in
745 at 425-475 nm; the Citrine signals were excited with the WLL at 495 nm, and obtained at 500-
746 530 nm with time gating (1.2-6.0 ns); the autofluorescence from chlorophyll was excited with
747 the WLL at 649 nm, and obtained at 655-755 nm.

748

749 **RNA extraction and qPCR**

750 For qPCR experiments, 50-100 mg of whole thallus was collected for each sample, which is
751 frozen with liquid nitrogen and crashed into fine powders with metal beads in a shaking device
752 (Shake Master Auto, BMS-A20TP, Bio Medical Science, Japan). The total RNA was extracted
753 with the TRIzol reagent (Thermo Fisher Scientific) following the manufacturer's protocol. After
754 treatment with RQ1 RNase-Free DNase (Promega), the total RNA was reverse-transcribed
755 using ReverTra Ace (Toyobo Life Science) and the $(dT)_{20}$ oligo. Quantitative real-time PCR
756 reactions with Taq polymerase prepared following (Pluthero, 1993) and SYBR Green I Nucleic
757 Acid Gel Stain (Lonza) was performed in triplicates using the CFX96 real-time PCR detection
758 system (Bio-Rad) with the following program: an initial denaturation for 30 s at 95 °C, then 40
759 cycles of 5 s at 95 °C followed by 30 s at 60 °C. A standard melting curve analysis was
760 performed at the end of the program to validate amplified products. Mp*EF1* (Mp3g23400) was
761 used as the reference gene for quantification, and the relative gene expression levels were
762 calculated following the method in (Hellemans et al., 2008). All primers for target and reference
763 genes were listed in Supplemental Table 3, and the amplification efficiency for each primer pair
764 was measured with serial dilution of mixed cDNA samples.

765

766 **Transcriptome analysis**

767 For transcriptome analysis, plants were cultured from gemmae on the medium with 1%
768 sucrose, either containing 2 μM KA or the solvent control. After 12 days of growth under cW or
769 cW+cFR, ~50 mg whole thallus was collected for each sample, frozen with liquid nitrogen and
770 homogenized with metal beads in a shaking device (Shake Master Auto, BMS-A20TP, Bio
771 Medical Science, Japan). The total RNA was isolated with the RNeasy Plant Mini Kit
772 (QIAGEN), and the RNA quality was confirmed using the Bioanalyzer RNA 6000 pico assay
773 (Agilent). The mRNA was enriched with the NEBNext Poly(A) mRNA Magnetic Isolation
774 Module (New England Biolabs, #E7490). The library was prepared with the NEBNext Ultra II
775 Directional RNA Library Prep Kit for Illumina (New England Biolabs, #E7760) and amplified
776 using NEBNext Multiplex Oligos for Illumina (96 Unique Dual Index Primer Pairs Set 2, New
777 England Biolabs, #E6442). After quality check with the Bioanalyzer High Sensitivity DNA assay
778 (Agilent), the samples were sequenced with the NextSeq 500 system using the NextSeq
779 500/550 High Output Kit v2.5 for 75 cycles (Illumina). Approximately 7.8 million of single-end
780 reads were obtained for each sample, and automatically de-multiplexed by the BaseSpace
781 Sequence Hub (Illumina).

782 The sequence reads were quasi-mapped to the *M. polymorpha* MpTak_v6.1 genome
783 (Iwasaki et al., 2021) and quantified using Salmon (v1.9.0) (Patro et al., 2017), with U-
784 chromosome transcripts excluded from the index. After that, differential gene expression
785 analysis was performed in R (v4.2.2) with the package DESeq2 (v1.38.3) in default settings
786 (Love et al., 2014). Gene ontology enrichment analyses was performed with the R package
787 topGO (v2.50.0) (Alexa and Rahnenfuhrer, 2022) using annotations previously described
788 (Hernández-García et al., 2021) and the classic Fisher's exact test, and *p*-values were left
789 unadjusted following the package's instructions. To visualize the enriched terms, semantic
790 similarities were calculated using the R package GOSemSim (v2.24.0) (Yu et al., 2010; Yu,
791 2020a), and used for building a two-dimensional map with the package Rtsne (Krijthe, 2015).
792 The transcriptome data is deposited to the Sequence Read Archive at the DNA Data Bank of
793 Japan (DDBJ) under the Bioproject PRJDB15786. The scripts for data analysis are available at
794 https://github.com/dorrenasun/Mp_GA_biosynthesis.

795

Supplemental Data

Supplemental Figure 1. Gibberellin (GA) biosynthesis pathway in vascular plants, showing compounds analyzed or used for treatment in this research.

Supplemental Figure 2. Genotype information for Mp*cps*^{ld}, Mp*ks*^{ld}, Mp*kol1*^{ld}, and Mp*kaol1*^{ge} mutants.

Supplemental Figure 3. Thallus morphology of Mp*cps*^{ld} mutants in Tak-2 background under cW+cFR.

Supplemental Figure 4. Morphology of Mp*cps*^{ld} plants during gametangiophore formation in the aseptic culture.

Supplemental Figure 5. Sections of gametangiophores in wild-type and Mp*cps*^{ld} plants, as well as the fertility test.

Supplemental Figure 6. LC-MS/MS and GC-MS profiles for KA and GA_{12} detection.

Supplemental Figure 7. Response of Mp*cps-4*^{ld} and Mp*kaol1-5*^{ge} to different concentrations of KA.

Supplemental Figure 8. Phylogenetic tree of KO homologs in land plants.

Supplemental Figure 9. Phylogenetic tree of KAO and closely-related CYP enzymes in land plants.

Supplemental Figure 10. Heatmap of percentage identity for KAO and closely-related CYP enzymes in land plants.

Supplemental Figure 11. Subcellular localizations of GA biosynthesis enzymes in *M. polymorpha*.

Supplemental Figure 12. Genotype information for Mp*tps1*^{ld}, [Mp*kol2* Mp*kol3*]^{ld} and Mp*kaol3*^{ld} mutants.

Supplemental Figure 13. Phenotypes of Mp*tps1*^{ld}, [Mp*kol2* Mp*kol3*]^{ld} and Mp*kaol3*^{ld} mutants.

Supplemental Figure 14. Up-regulation of GA biosynthesis genes by FR irradiation.

Supplemental Figure 15. Heatmaps of genes from selected pathways or gene families, showing differential expression in Mp*cps-4*^{ld} under cW+cFR.

Supplemental Figure 16. Quantification method for thallus morphology.

Supplemental Table 1. List of plant materials

Supplemental Table 2. List of plasmids

827 **Supplemental Table 3**. List of DNA oligos
828 **Supplemental Data Set 1**. Differentially expressed genes in the transcriptome analysis
829 **Supplemental Data Set 2**. Enriched gene ontology (GO) terms in the transcriptome
830 analysis
831 **Supplemental Data Set 3**. List of genome and transcriptome sources for phylogenetic
832 analysis
833
834 **Supplemental References**.
835

836 **AKNOWLEDGEMENTS**

837 The authors thank Ryunosuke Kusunoki for plasmid construction and collecting initial
838 experimental data; Wakako Fukuda for data collection during GC-MS analysis; Takefumi
839 Kondo and Yukari Sando for the support on RNA sequencing; Megumi Iwano for the help on
840 confocal microscopy and Chikako Inoue for plant maintenance. This work has been supported
841 by MEXT KAKENHI Grant Number JP19H05675 and JSPS KAKENHI Grant Numbers
842 JP17H07424, JP22H00417 to T.K.; JSPS KAKENHI Grant Numbers JP 24380060,
843 JP15H04492 to M.N. and H.K.; JSPS KAKENHI Grant Number JP16K18693 to S.M.; as well
844 as the International Collaborative Research Program of Institute for Chemical Research, Kyoto
845 University (Grant Numbers 2020-53, 2021-60, 2022-63, 2023-74) to T.K. and S.Yamaguchi.
846

847 **AUTHOR CONTRIBUTIONS**

848 R.S. and M.O. collected and analyzed most of the final data with the help and supervision
849 from K.M., Y.Y., S.Yamaoka., R.N. and T.K.. M.O., S.M., T.I., K.M., M.N. and S.Yamaguchi
850 analyzed endogenous GAs. S.M. and H.K. assayed enzymatic activity. R.K. performed initial
851 experiments that conceptualized the research. H.K., M.N., S.Yamaguchi and T.K. organized
852 the project. R.S., S.Yamaoka., R.N and T.K. wrote the paper with the review and editing from
853 all authors.
854

855 **REFERENCES**

856 Achard, P., Gusti, A., Cheminant, S., Alioua, M., Dhondt, S., Coppens, F., Beemster, G.T.S.,
857 and Genschik, P. (2009). Gibberellin Signaling Controls Cell Proliferation Rate in
858 Arabidopsis. Current Biology 19: 1188–1193.

Aki, S.S., Mikami, T., Naramoto, S., Nishihama, R., Ishizaki, K., Kojima, M., Takebayashi, Y., Sakakibara, H., Kyozuka, J., Kohchi, T., and Umeda, M. (2019). Cytokinin Signaling Is Essential for Organ Formation in Marchantia polymorpha. Plant and Cell Physiology 60: 1842–1854.

Alexa, A. and Rahnenfuhrer, J. (2022). topGO: Enrichment Analysis for Gene Ontology. R package version 2.50.0.

Althoff, F., Kopischke, S., Zobell, O., Ide, K., Ishizaki, K., Kohchi, T., and Zachgo, S. (2014). Comparison of the MpEF1α and CaMV35 promoters for application in Marchantia polymorpha overexpression studies. Transgenic Res 23: 235–244.

Altschul, S.F., Gish, W., Miller, W., Myers, E.W., and Lipman, D.J. (1990). Basic local alignment search tool. Journal of Molecular Biology 215: 403–410.

Beall, F.D., Yeung, E.C., and Pharis, R.P. (1996). Far-red light stimulates internode elongation, cell division, cell elongation, and gibberellin levels in bean. Can. J. Bot. 74: 743–752.

Bou-Torrent, J., Galstyan, A., Gallemí, M., Cifuentes-Esquivel, N., Molina-Contreras, M.J., Salla-Martret, M., Jikumaru, Y., Yamaguchi, S., Kamiya, Y., and Martínez-García, J.F. (2014). Plant proximity perception dynamically modulates hormone levels and sensitivity in Arabidopsis. Journal of Experimental Botany 65: 2937–2947.

Bowman, J.L. et al. (2017). Insights into land plant evolution garnered from the *Marchantia polymorpha* genome. Cell 171: 287-304.e15.

Briginshaw, L.N., Flores-Sandoval, E., Dierschke, T., Alvarez, J.P., and Bowman, J.L. (2022). KANADI promotes thallus differentiation and FR-induced gametangiophore formation in the liverwort Marchantia. New Phytologist 234: 1377–1393.

Cannell, N., Emms, D.M., Hetherington, A.J., MacKay, J., Kelly, S., Dolan, L., and Sweetlove, L.J. (2020). Multiple Metabolic Innovations and Losses Are Associated with Major Transitions in Land Plant Evolution. Current Biology 30: 1783-1800.e11.

Cao, J.-G., Wang, Q.-X., Zou, H.-M., Dai, X.-L., and Cao, T. (2013). New Observations on the Morphology and Structure of *Marchantia polymorpha* Gametophores in Sexual Reproduction Adaption. Plant Science Journal 31: 555.

Chiang, H.-H., Hwang, I., and Goodman, H.M. (1995). Isolation of the Arabidopsis *GA4* locus. the Plant Cell 7: 195–201.

Chiyoda, S., Ishizaki, K., Kataoka, H., Yamato, K.T., and Kohchi, T. (2008). Direct transformation of the liverwort Marchantia polymorpha L. by particle bombardment using immature thalli developing from spores. Plant Cell Reports 27: 1467–1473.

Conesa, A. and Götz, S. (2008). Blast2GO: A comprehensive suite for functional analysis in plant genomics. International Journal of Plant Genomics 2008.

894 Djakovic-Petrovic, T., Wit, M.D., Voesenek, L.A.C.J., and Pierik, R. (2007). DELLA protein
895 function in growth responses to canopy signals. Plant Journal 51: 117–126.

896 Downs, R.J., Hendricks, S.B., and Borthwick, H.A. (1957). Photoreversible Control of
897 Elongation of Pinto Beans and Other Plants under Normal Conditions of Growth.
898 Botanical Gazette 118: 199–208.

899 Dubois, P.G., Olsefski, G.T., Flint-Garcia, S., Setter, T.L., Hoekenga, O.A., and Brutnell, T.P.
900 (2010). Physiological and Genetic Characterization of End-of-Day Far-Red Light
901 Response in Maize Seedlings. Plant Physiology 154: 173–186.

902 Fredericq, H. (1964). Influence formatrice de la lumière rouge-foncé sur le développement des
903 thalles de Marchantia polymorpha L. Bull. Soc. Roy. Bot. Belgique 98: 67–76.

904 Fredericq, H. and de Greef, J. (1966). Red (R), Far-red (FR) photoreversible control of growth
905 and chlorophyll content in light-grown thalli of Marchantia polymorpha L. Die
906 Naturwissenschaften 53: 337.

907 Fredericq, H. and Greef, J.D. (1968). Photomorphogenic and Chlorophyll Studies in the
908 Bryophyte Marchantia polymorpha. I. Effect of Red, Far-red Irradiations in Short and
909 Long-term Experiments. Physiol Plant 21: 346–359.

910 Gabriele, S., Rizza, A., Martone, J., Circelli, P., Costantino, P., and Vittorioso, P. (2009). The
911 Dof protein DAG1 mediates PIL5 activity on seed germination by negatively regulating
912 GA biosynthetic gene AtGA3ox1: DAG1 represses seed germination via PIL5 signalling.
913 The Plant Journal 61: 312–323.

914 Gamborg, O.L., Miller, R.A., and Ojima, K. (1968). Nutrient requirements of suspension
915 cultures of soybean root cells. Experimental Cell Research 50: 151–158.

916 García-Martínez, J.L., Keith, B., Bonner, B.A., Stafford, A.E., and Rappaport, L. (1987).
917 Phytochrome Regulation of the Response to Exogenous Gibberellins by Epicotyls of
918 *Vigna sinensis*. Plant Physiol. 85: 212–216.

919 Guindon, S., Dufayard, J.-F., Lefort, V., Anisimova, M., Hordijk, W., and Gascuel, O. (2010).
920 New algorithms and methods to estimate maximum-likelihood phylogenies: Assessing
921 the performance of PhyML 3.0. Systematic Biology 59: 307–321.

922 Hayashi, K., Horie, K., Hiwatashi, Y., Kawaide, H., Yamaguchi, S., Hanada, A., Nakashima, T.,
923 Nakajima, M., Mander, L.N., Yamane, H., Hasebe, M., and Nozaki, H. (2010).
924 Endogenous diterpenes derived from *ent*-kaurene, a common gibberellin precursor,
925 regulate protonema differentiation of the moss *Physcomitrella patens*. Plant Physiology
926 153: 1085–1097.

927 Hayashi, K. ichiro, Kawaide, H., Notomi, M., Sakigi, Y., Matsuo, A., and Nozaki, H. (2006).
928 Identification and functional analysis of bifunctional *ent*-kaurene synthase from the moss
929 *Physcomitrella patens*. FEBS Letters 580: 6175–6181.

Hedden, P. (2020). The Current Status of Research on Gibberellin Biosynthesis. Plant and Cell Physiology 61: 1832–1849.

Hedden, P., MacMillan, J., and Phinney, B.O. (1974). Fungal products. Part XII. Gibberellin A14-aldehyde, an intermediate in gibberellin biosynthesis in Gibberella fujikuroi. Journal of the Chemical Society, Perkin Transactions 1: 587–592.

Hellemans, J., Mortier, G., De Paepe, A., Speleman, F., and Vandesompele, J. (2008). qBase relative quantification framework and software for management and automated analysis of real-time quantitative PCR data. Genome Biology 8.

Helliwell, C.A., Chandler, P.M., Poole, A., Dennis, E.S., and Peacock, W.J. (2001a). The CYP88A cytochrome P450, *ent*-kaurenoic acid oxidase, catalyzes three steps of the gibberellin biosynthesis pathway. Proceedings of the National Academy of Sciences of the United States of America 98: 2065–2070.

Helliwell, C.A., Poole, A., James Peacock, W., and Dennis, E.S. (1999). Arabidopsis *ent* -kaurene oxidase catalyzes three steps of gibberellin biosynthesis. Plant Physiology 119: 507–510.

Helliwell, C.A., Sheldon, C.C., Olive, M.R., R.Walker, A., Zeevaart, J.A.D., Peacock, W.J., and Dennis, E.S. (1998). Cloning of the *Arabidopsis ent*-kaurene oxidase gene *GA3*. Proceedings of the National Academy of Sciences of the United States of America 95: 9019–9024.

Helliwell, C.A., Sullivan, J.A., Mould, R.M., Gray, J.C., James Peacock, W., and Dennis, E.S. (2001b). A plastid envelope location of *Arabidopsis ent*-kaurene oxidase links the plastid and endoplasmic reticulum steps of the gibberellin biosynthesis pathway. Plant Journal 28: 201–208.

Hernández-García, J., Sun, R., Serrano-Mislata, A., Inoue, K., Vargas-Chávez, C., Esteve-Bruna, D., Arbona, V., Yamaoka, S., Nishihama, R., Kohchi, T., and Blázquez, M.A. (2021). Coordination between growth and stress responses by DELLA in the liverwort Marchantia polymorpha. Current Biology.

Hirano, K. et al. (2007). The GID1-mediated gibberellin perception mechanism is conserved in the lycophyte Selaginella moellendorffii but not in the bryophyte *Physcomitrella patens*. The Plant Cell 19: 3058–3079.

Hisamatsu, T., King, R.W., Helliwell, C. a, and Koshioka, M. (2005). The involvement of gibberellin 20-oxidase genes in phytochrome-regulated petiole elongation of Arabidopsis. Plant Physiology 138: 1106–1116.

Hisanaga, T., Okahashi, K., Yamaoka, S., Kajiwara, T., Nishihama, R., Shimamura, M., Yamato, K.T., Bowman, J.L., Kohchi, T., and Nakajima, K. (2019). A cis -acting bidirectional transcription switch controls sexual dimorphism in the liverwort. The EMBO Journal 38: 1–12.

Hoang, D.T., Chernomor, O., von Haeseler, A., Minh, B.Q., and Vinh, L.S. (2018). UFBoot2: Improving the Ultrafast Bootstrap Approximation. Molecular Biology and Evolution 35: 518–522.

Holmes, M.G. and Smith, H. (1975). The function of phytochrome in plants growing in the natural environment. Nature 254: 512–514.

Hornych, O., Testo, W.L., Sessa, E.B., Watkins, J.E., Campany, C.E., Pittermann, J., and Ekrt, L. (2021). Insights into the evolutionary history and widespread occurrence of antheridiogen systems in ferns. New Phytologist 229: 607–619.

Inoue, K., Nishihama, R., Araki, T., and Kohchi, T. (2019). Reproductive induction is a far-red high irradiance response that is mediated by phytochrome and PHYTOCHROME INTERACTING FACTOR in Marchantia polymorpha. Plant and Cell Physiology 60: 1136–1145.

Inoue, K., Nishihama, R., Kataoka, H., Hosaka, M., Manabe, R., Nomoto, M., Tada, Y., Ishizaki, K., and Kohchi, T. (2016). Phytochrome signaling is mediated by PHYTOCHROME INTERACTING FACTOR in the liverwort *Marchantia polymorpha*. The Plant Cell 28: 1406–1421.

Ishizaki, K., Chiyoda, S., Yamato, K.T., and Kohchi, T. (2008). *Agrobacterium*-mediated transformation of the haploid liverwort *Marchantia polymorpha* L., an emerging model for plant biology. Plant and Cell Physiology 49: 1084–1091.

Ishizaki, K., Nishihama, R., Ueda, M., Inoue, K., Ishida, S., Nishimura, Y., Shikanai, T., and Kohchi, T. (2015). Development of Gateway binary vector series with four different selection markers for the liverwort *Marchantia polymorpha*. PLoS ONE 10: e0138876.

Iwasaki, M. et al. (2021). Identification of the sex-determining factor in the liverwort Marchantia polymorpha reveals unique evolution of sex chromosomes in a haploid system. Current Biology 31: 5522-5532.e7.

Jia, Q., Brown, R., Köllner, T.G., Fu, J., Chen, X., Wong, G.K.S., Gershenzon, J., Peters, R.J., and Chen, F. (2022). Origin and early evolution of the plant terpene synthase family. Proceedings of the National Academy of Sciences of the United States of America 119: 1–9.

Kalyaanamoorthy, S., Minh, B.Q., Wong, T.K.F., von Haeseler, A., and Jermiin, L.S. (2017). ModelFinder: fast model selection for accurate phylogenetic estimates. Nat Methods 14: 587–589.

Katoh, K. and Standley, D.M. (2013). MAFFT multiple sequence alignment software version 7: Improvements in performance and usability. Molecular Biology and Evolution 30: 772–780.

Katsumata, T., Hasegawa, A., Fujiwara, T., Komatsu, T., Notomi, M., Abe, H., Natsume, M., and Kawaide, H. (2008). Arabidopsis CYP85A2 Catalyzes Lactonization Reactions in

the Biosynthesis of 2-Deoxy-7-oxalactone Brassinosteroids. Bioscience, Biotechnology, and Biochemistry 72: 2110–2117.

Kohnen, M.V., Schmid-Siegert, E., Trevisan, M., Petrolati, L.A., Sénéchal, F., Müller-Moulé, P., Maloof, J., Xenarios, I., and Fankhauser, C. (2016). Neighbor Detection Induces Organ-Specific Transcriptomes, Revealing Patterns Underlying Hypocotyl-Specific Growth. Plant Cell 28: 2889–2904.

Koide, E., Suetsugu, N., Iwano, M., Gotoh, E., Nomura, Y., Stolze, S.C., Nakagami, H., Kohchi, T., and Nishihama, R. (2020). Regulation of Photosynthetic Carbohydrate Metabolism by a Raf-Like Kinase in the Liverwort Marchantia polymorpha. Plant and Cell Physiology 61: 631–643.

Koornneef, M. and van der Veen, J.H. (1980). Induction and analysis of gibberellin sensitive mutants in *Arabidopsis thaliana* (L.) heynh. Theoretical and Applied Genetics 58: 257–263.

Krijthe, J.H. (2015). Rtsne: T-Distributed Stochastic Neighbor Embedding using a Barnes-Hut Implementation.

Kubota, A., Ishizaki, K., Hosaka, M., and Kohchi, T. (2013). Efficient *Agrobacterium*-mediated transformation of the liverwort *Marchantia polymorpha* using regenerating thalli. Bioscience, Biotechnology and Biochemistry 77: 167–172.

Kumar, S. et al. (2016). Molecular diversity of terpene synthases in the liverwort *Marchantia polymorpha*. The Plant Cell 28: 2632–2650.

Küpers, J.J. et al. (2023). Local light signaling at the leaf tip drives remote differential petiole growth through auxin-gibberellin dynamics. Current Biology 33: 75-85.e5.

Kurihara, D., Mizuta, Y., Nagahara, S., and Higashiyama, T. (2021). ClearSeeAlpha: Advanced Optical Clearing for Whole-Plant Imaging. Plant and Cell Physiology 62: 1302–1310.

Kurosawa, E. (1926). Experimental studies on the nature of the substance excreted by the “bakanae” fungus. Trans. Nat. Hist. Soc. Formosa 16: 213–227.

Li, W., Liu, S.-W., Ma, J.-J., Liu, H.-M., Han, F.-X., Li, Y., and Niu, S.-H. (2020). Gibberellin Signaling Is Required for Far-Red Light-Induced Shoot Elongation in *Pinus tabuliformis* Seedlings. Plant Physiol. 182: 658–668.

Love, M.I., Huber, W., and Anders, S. (2014). Moderated estimation of fold change and dispersion for RNA-seq data with DESeq2. Genome Biology 15: 550.

Michaud, O., Krahmer, J., Galbier, F., Lagier, M., Galvão, V.C., Ince, Y.Ç., Trevisan, M., Knerova, J., Dickinson, P., Hibberd, J.M., Zeeman, S.C., and Fankhauser, C. (2023). Abscisic acid modulates neighbor proximity-induced leaf hyponasty in Arabidopsis. Plant Physiology 191: 542–557.

1039 Minh, B.Q., Schmidt, H.A., Chernomor, O., Schrempf, D., Woodhams, M.D., von Haeseler, A.,
1040 and Lanfear, R. (2020). IQ-TREE 2: New Models and Efficient Methods for Phylogenetic
1041 Inference in the Genomic Era. Molecular Biology and Evolution 37: 1530–1534.

1042 Miyazaki, S., Hara, M., Ito, S., Tanaka, K., Asami, T., Hayashi, K., Kawaide, H., and Nakajima,
1043 M. (2018). An Ancestral Gibberellin in a Moss Physcomitrella patens. Molecular Plant
1044 11: 1097–1100.

1045 Miyazaki, S., Katsumata, T., Natsume, M., and Kawaide, H. (2011). The CYP701B1 of
1046 *Physcomitrella patens* is an ent-kaurene oxidase that resists inhibition by uniconazole-P.
1047 FEBS Letters 585: 1879–1883.

1048 Miyazaki, S., Nakajima, M., and Kawaide, H. (2015). Hormonal diterpenoids derived from ent-
1049 kaurenoic acid are involved in the blue-light avoidance response of Physcomitrella
1050 patens. Plant Signaling and Behavior 10: 1–4.

1051 Miyazaki, S., Toyoshima, H., Natsume, M., Nakajima, M., and Kawaide, H. (2014). Blue-light
1052 irradiation up-regulates the *ent*-kaurene synthase gene and affects the avoidance
1053 response of protonemal growth in *Physcomitrella patens*. Planta 240: 117–124.

1054 Morgan, D.C. and Smith, H. (1979). A systematic relationship between phytochrome-controlled
1055 development and species habitat, for plants grown in simulated natural radiation. Planta
1056 145: 253–258.

1057 Morgan, D.C. and Smith, H. (1978). The relationship between phytochrome-photoequilibrium
1058 and Development in light grown Chenopodium album L. Planta 142: 187–193.

1059 Motohashi, K. (2015). A simple and efficient seamless DNA cloning method using SLiCE from
1060 Escherichia coli laboratory strains and its application to SLiP site-directed mutagenesis.
1061 BMC Biotechnol 15: 47.

1062 Näf, U., Nakanishi, K., and Endo, M. (1975). On the Physiology and Chemistry of Fern
1063 Antheridiogens. Botanical Review 41: 315–359.

1064 Nelissen, H., Rymen, B., Jikumaru, Y., Demuynck, K., Van Lijsebettens, M., Kamiya, Y., Inzé,
1065 D., and Beemster, G.T.S. (2012). A Local Maximum in Gibberellin Levels Regulates
1066 Maize Leaf Growth by Spatial Control of Cell Division. Current Biology 22: 1183–1187.

1067 Ninnemann, H. and Halbsguth, W. (1965). Rolle des Phytochroms beim Etiolement von
1068 Marchantia polymorpha. Naturwissenschaften 52: 110–111.

1069 Nomura, T., Magome, H., Hanada, A., Takeda-Kamiya, N., Mander, L.N., Kamiya, Y., and
1070 Yamaguchi, S. (2013). Functional analysis of *Arabidopsis* CYP714A1 and CYP714A2
1071 reveals that they are distinct gibberellin modification enzymes. Plant and Cell
1072 Physiology 54: 1837–1851.

1073 Ogawa, M., Hanada, A., Yamauchi, Y., Kuwahara, A., Kamiya, Y., and Yamaguchi, S. (2003).
1074 Gibberellin Biosynthesis and Response during Arabidopsis Seed Germination. The
1075 Plant Cell 15: 1591–1604.

1076 Patro, R., Duggal, G., Love, M.I., Irizarry, R.A., and Kingsford, C. (2017). Salmon provides fast
1077 and bias-aware quantification of transcript expression. Nature Methods 14: 417–419.

1078 Pluthero, F.G. (1993). Rapid purification of high-activity Taq DNA polymerase. Nucleic Acids
1079 Res 21: 4850–4851.

1080 Rojas, M.C., Hedden, P., Gaskin, P., and Tudzynski, B. (2001). The *P450–1* gene of
1081 *Gibberella fujikuroi* encodes a multifunctional enzyme in gibberellin biosynthesis. Proc.
1082 Natl. Acad. Sci. U.S.A. 98: 5838–5843.

1083 Sakamoto, Y., Ishimoto, A., Sakai, Y., Sato, M., Nishihama, R., Abe, K., Sano, Y., Furuichi, T.,
1084 Tsuji, H., Kohchi, T., and Matsunaga, S. (2022). Improved clearing method contributes
1085 to deep imaging of plant organs. Commun Biol 5: 12.

1086 Schindelin, J. et al. (2012). Fiji: an open-source platform for biological-image analysis. Nat
1087 Methods 9: 676–682.

1088 Schmidt, U., Weigert, M., Broaddus, C., and Myers, G. (2018). Cell Detection with Star-Convex
1089 Polygons. In Medical Image Computing and Computer Assisted Intervention – MICCAI
1090 2018, A.F. Frangi, J.A. Schnabel, C. Davatzikos, C. Alberola-López, and G. Fichtinger,
1091 eds, Lecture Notes in Computer Science. (Springer International Publishing: Cham), pp.
1092 265–273.

1093 Schneller, J.J. (2008). Antheridiogens. In Biology and Evolution of Ferns and Lycophytes, T.A.
1094 Ranker and C.H. Haufler, eds (Cambridge University Press: New York), pp. 134–158.

1095 Sessa, G., Carabelli, M., Sassi, M., Ciolfi, A., Possenti, M., Mittempergher, F., Becker, J.,
1096 Morelli, G., and Ruberti, I. (2005). A dynamic balance between gene activation and
1097 repression regulates the shade avoidance response in *Arabidopsis*. Genes Dev. 19:
1098 2811–2815.

1099 Shimamura, M. (2016). *Marchantia polymorpha*: Taxonomy, phylogeny and morphology of a
1100 model system. Plant and Cell Physiology 57: 230–256.

1101 Sponsel, V.M. (2016). Signal achievements in gibberellin research: the second half-century.
1102 Annual Plant Reviews: The Gibberellins 49: 1–36.

1103 Streubel, S., Deiber, S., Rötzer, J., Mosiolek, M., Jandrasits, K., and Dolan, L. (2023).
1104 Meristem dormancy in Marchantia polymorpha is regulated by a liverwort-specific
1105 miRNA and a clade III SPL gene. Current Biology: S0960982222019996.

1106 Sugano, S.S., Nishihama, R., Shirakawa, M., Takagi, J., Matsuda, Y., Ishida, S., Shimada, T.,
1107 Hara-Nishimura, I., Osakabe, K., and Kohchi, T. (2018). Efficient CRISPR/Cas9-based

genome editing and its application to conditional genetic analysis in Marchantia polymorpha. PLoS ONE 13: e0205117.

Sun, T. and Kamiya, Y. (1994). The Arabidopsis *GA1* locus encodes the cyclase *ent*-kaurene synthetase A of gibberellin biosynthesis. the Plant Cell 6: 1509–1518.

Talon, M., Koornneef, M., and Zeevaart, J.A.D. (1990). Endogenous gibberellins in Arabidopsis thaliana and possible steps blocked in the biosynthetic pathways of the semidwarf ga4 and ga5 mutants. Proceedings of the National Academy of Sciences of the United States of America 87: 7983–7987.

Tanaka, J., Yano, K., Aya, K., Hirano, K., Takehara, S., Koketsu, E., Ordonio, R.L., Park, S.-H., Nakajima, M., Ueguchi-Tanaka, M., and Matsuoka, M. (2014). Antheridiogen determines sex in ferns via a spatiotemporally split gibberellin synthesis pathway. Science 346: 469–473.

Toyomasu, T., Kawaide, H., Mitsuhashi, W., Inoue, Y., and Kamiya, Y. (1998). Phytochrome regulates gibberellin biosynthesis during germination of photoblastic lettuce seeds. Plant Physiology 118: 1517–1523.

Ubeda-Tomás, S., Federici, F., Casimiro, I., Beemster, G.T.S., Bhalerao, R., Swarup, R., Doerner, P., Haseloff, J., and Bennett, M.J. (2009). Gibberellin Signaling in the Endodermis Controls Arabidopsis Root Meristem Size. Current Biology 19: 1194–1199.

Ubeda-Tomás, S., Swarup, R., Coates, J., Swarup, K., Laplaze, L., Beemster, G.T.S., Hedden, P., Bhalerao, R., and Bennett, M.J. (2008). Root growth in Arabidopsis requires gibberellin/DELLA signalling in the endodermis. Nat Cell Biol 10: 625–628.

Urrutia, O., Hedden, P., and Rojas, M.C. (2001). Monooxygenases involved in GA12 and GA14 synthesis in Gibberella fujikuroi. Phytochemistry 56: 505–511.

Van Tuinen, A., Peters, A.H.L.J., Kendrick, R.E., Zeevaart, J. a. D., and Koornneef, M. (1999). Characterisation of the procera mutant of tomato and the interaction of gibberellins with end-of-day far-red light treatments. Physiologia Plantarum 106: 121–128.

Wenzel, C.L., Williamson, R.E., and Wasteneys, G.O. (2000). Gibberellin-Induced Changes in Growth Anisotropy Precede Gibberellin-Dependent Changes in Cortical Microtubule Orientation in Developing Epidermal Cells of Barley Leaves. Kinematic and Cytological Studies on a Gibberellin-Responsive Dwarf Mutant, M489. Plant Physiology 124: 813–822.

Whitelam, G.C. and Johnson, C.B. (1982). PHOTOMORPHOGENESIS IN IMPATIENS PARVIFLORA AND OTHER PLANT SPECIES UNDER SIMULATED NATURAL CANOPY RADIATIONS. New Phytol 90: 611–618.

Whitelam, G.C. and Smith, H. (1991). Retention of Phytochrome-Mediated Shade Avoidance Responses in Phytochrome-Deficient Mutants of Arabidopsis, Cucumber and Tomato. Journal of Plant Physiology 139: 119–125.

Williams, J., Phillips, A.L., Gaskin, P., and Hedden, P. (1998). Function and Substrate Specificity of the Gibberellin 3β-Hydroxylase Encoded by the Arabidopsis GA4Gene. Plant Physiology 117: 559–563.

Xu, S., Li, L., Luo, X., Chen, M., Tang, W., Zhan, L., Dai, Z., Lam, T.T., Guan, Y., and Yu, G. (2022). Ggtree: A serialized data object for visualization of a phylogenetic tree and annotation data. iMeta 1: e56.

Yamaguchi, S., Smith, M.W., Brown, R.G.S., Kamiya, Y., and Sun Tai-ping (1998a). Phytochrome Regulation and Differential Expression of Gibberellin 3β-Hydroxylase Genes in Germinating Arabidopsis Seeds. The Plant Cell 10: 2115–2126.

Yamaguchi, S., Sun, T., Kawaide, H., and Kamiya, Y. (1998b). The *GA2* locus of *Arabidopsis thaliana* encodes *ent*-kaurene synthase of gibberellin biosynthesis. Plant Physiology 116: 1271–1278.

Yamane, H. (1998). Fern Antheridiogens. International Review of Cytology 184: 1–32.

Yamaoka, S. et al. (2018). Generative Cell Specification Requires Transcription Factors Evolutionarily Conserved in Land Plants. Current Biology 28: 479-486.e5.

Yamauchi, T., Oyama, N., Yamane, H., Murofushi, N., Schraudolf, H., Pour, M., Furber, M., and Mander, L.N. (1996). Identification of Antheridiogens in Lygodium circinnatum and Lygodium flexuosum. Plant Physiology 111: 741–745.

Yoshida, H., Takehara, S., Mori, M., Ordonio, R.L., and Matsuoka, M. (2020). Evolution of GA metabolic enzymes in land plants. Plant and Cell Physiology 61: 1919–1934.

Yu, G. (2022). Data Integration, Manipulation and Visualization of Phylogenetic Trees (Chapman and Hall/CRC: New York).

Yu, G. (2020a). Gene ontology semantic similarity analysis using GOSemSim. In Methods in Molecular Biology (Humana Press Inc.), pp. 207–215.

Yu, G. (2020b). Using ggtree to Visualize Data on Tree-Like Structures. Current Protocols in Bioinformatics 69: e96.

Yu, G., Lam, T.T.-Y., Zhu, H., and Guan, Y. (2018). Two Methods for Mapping and Visualizing Associated Data on Phylogeny Using Ggtree. Molecular Biology and Evolution 35: 3041–3043.

Yu, G., Li, F., Qin, Y., Bo, X., Wu, Y., and Wang, S. (2010). GOSemSim: an R package for measuring semantic similarity among GO terms and gene products. Bioinformatics 26: 976–978.

Yu, G., Smith, D.K., Zhu, H., Guan, Y., and Lam, T.T.-Y. (2017). ggtree: an r package for visualization and annotation of phylogenetic trees with their covariates and other associated data. Methods in Ecology and Evolution 8: 28–36.

1180 Zhang, Y., Werling, U., and Edelmann, W. (2012). SLiCE: A novel bacterial cell extract-based
1181 DNA cloning method. Nucleic Acids Research 40: 1–10.

1182

1183

Main Figures

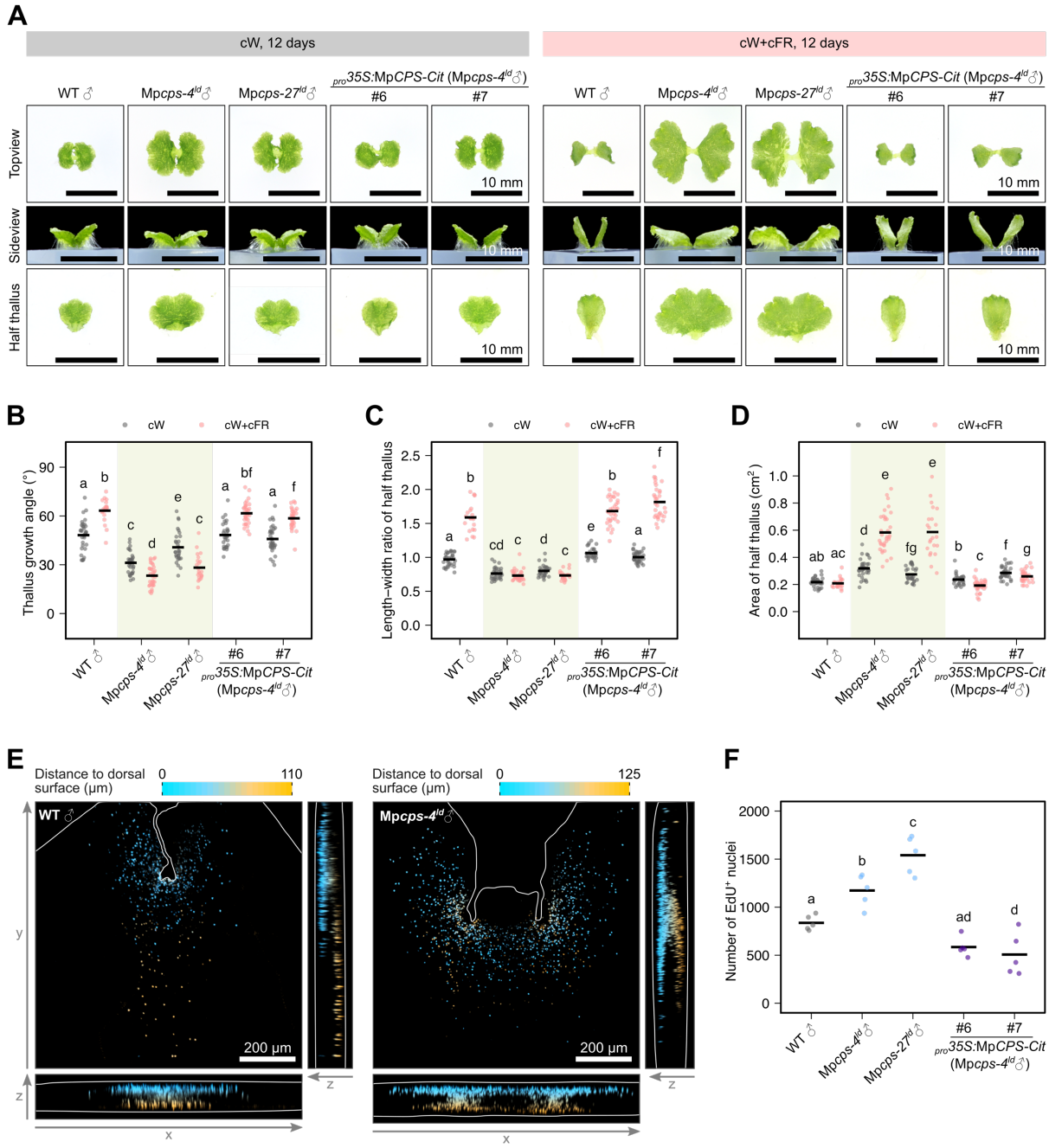

Figure 1 Loss of Mp*CPS* activity alters thallus morphology under far-red light (FR) enriched conditions. A, Morphology of 12-day-old plants grown from gemmae under continuous white light (cW) or continuous white light with far-red light (cW+cFR) conditions. Images were selected randomly from different plants. Bars = 10 mm. B-D, Measurements of the thallus growth angle (B), length-width ratio (C) and thallus area (D) from half plants shown in A. n=21-36. E, Apical regions of plants labelled with 5-ethynyl-2'-deoxyuridine (EdU) after 7-day growth in cW+cFR, showing two-dimensional projections of color-coded z-stacks. White lines mark the boundary of plants or imaging area. F, Number of nuclei with positive EdU signals in the apical regions of 7-day-old plants grown in cW+cFR (n=5). For all figures, WT♂ refer to Tak-1 wild-type plants. For B-D and F, each dot represents data from a "half thallus", which was developed from a single meristem of the gemma. Horizontal lines represent mean values. Letters represent statistical differences, and groups with no common letters were significantly different (adjusted $p<0.05$). For B-D, non-pooled Welch's *t*-test with Benjamini-Hochberg (B-H) adjustment was used due to heterogeneity of variance. Tukey's HSD test was used in F.

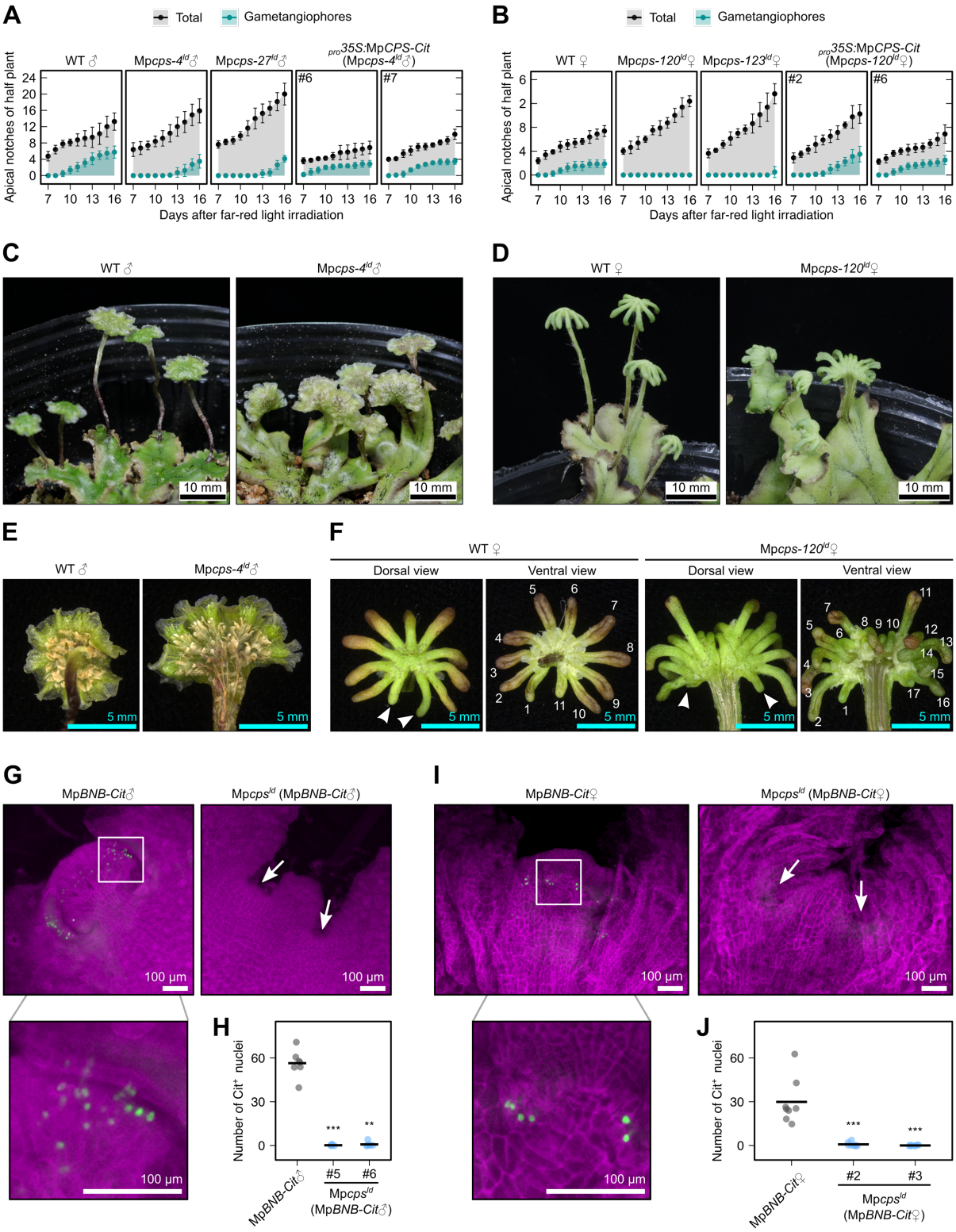
A
Total
Gametangiophores
WT ♂
Mpcps-4ld♂
Mpcps-27ld♂
proMp35S:MpCPS-Cit (Mpcps-4ld♂)
#6
#7
Apical notches of half plant
Days after far-red light irradiation
B
WT ♀
Mpcps-120ld♀
Mpcps-123ld♀
proMp35S:MpCPS-Cit (Mpcps-120ld♀)
#2
#6
C
WT ♂
Mpcps-4ld♂
10 mm
D
WT ♀
Mpcps-120ld♀
10 mm
E
WT ♂
Mpcps-4ld♂
5 mm
F
WT ♀
Mpcps-120ld♀
Dorsal view
Ventral view
5 mm
G
MpBNB-Cit♂
Mpcpsld (MpBNB-Cit♂)
100 µm
H
Number of Cit+ nuclei
MpBNB-Cit♂
#5
#6
Mpcpsld (MpBNB-Cit♂)
I
MpBNB-Cit♀
Mpcpsld (MpBNB-Cit♀)
J
MpBNB-Cit♀
#2
#3
Mpcpsld (MpBNB-Cit♀)

Figure 2 Mp*CPS* is required for delayed sexual reproduction and affected gametangiophore morphology.

A-B, Progress of apical bifurcation and gametangiophore formation in male (A) and female (B) plants, which were cultured aseptically under cW for 7 days before transferred to cW+cFR. Dots and error bars represent means and standard deviations, respectively. n=8. WT♂ and WT♀ refer to Tak-1 and Tak-2 wild-type plants, respectively. C-D, Photos of male (C) and female (D) plants bearing gametangiophores, cultured on vermiculite under cW+cFR from thallus fragments for 81 and 63 days, respectively. E, Ventral view of antheridiophores. F, Dorsal and ventral view of archegoniophores. Arrowheads indicate marginal digitate rays, and the number of digitate rays was labeled in the ventral view. G-J, Fluorescence microscopic images and quantification of MpBNB-Cit accumulation in the apical regions of 11-day-old male (G-H, dorsal view), or 14-day-old female (I-J, ventral view) plants cultured under cW+cFR from gemmae. G and I, Z-projections of image stacks, with cell walls stained with calcofluor white (purple) and Citrine signals shown in green. Arrows indicate apical meristems. H and J, Number of Citrine-positive nuclei counted from projection of image stacks. Each dot represents data from 1/2 (H) or 1/4 (J) of the thallus, and horizontal lines represent mean values. Asterisks show statistical difference compared to the control group (Mann-Whitney *U* test; **, $p<0.01$; ***, $p<0.001$). n=7 for H, n=8 for J.

A

Metabolite	Endogenous Level	Metabolite	Endogenous Level
GA_1	not detected	GA_{20}	not detected
GA_4	not detected	GA_{24}	not detected
GA_8	not detected	GA_{29}	not detected
GA_9	not detected	GA_{34}	not detected
GA_{12}	28.9±6.5	GA_{44}	not detected
GA_{15}	not detected	GA_{51}	not detected
GA_{19}	not detected	GA_{53}	not detected

(unit: pg/g fresh weight)

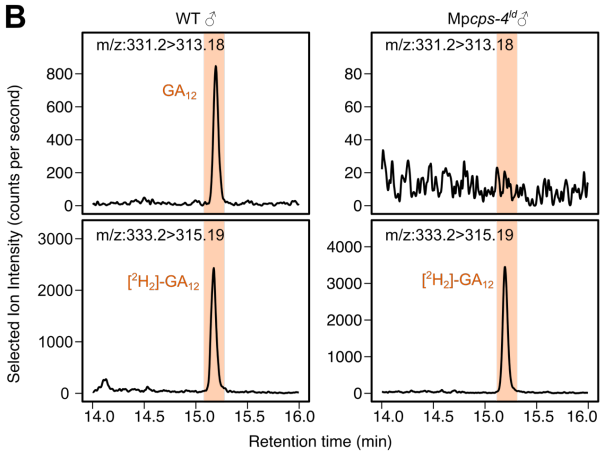

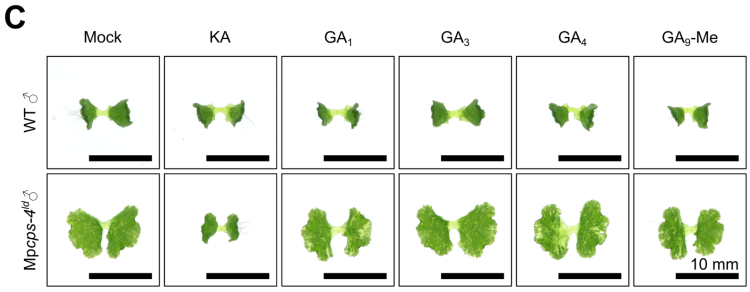

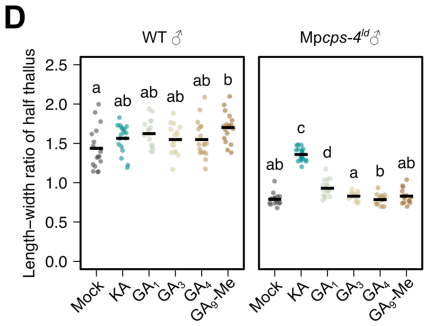

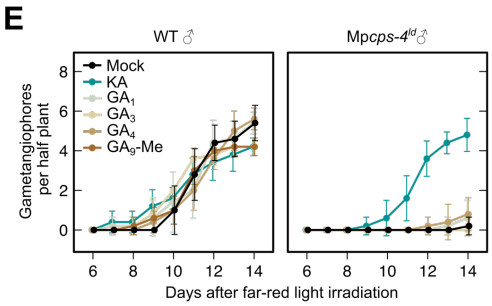

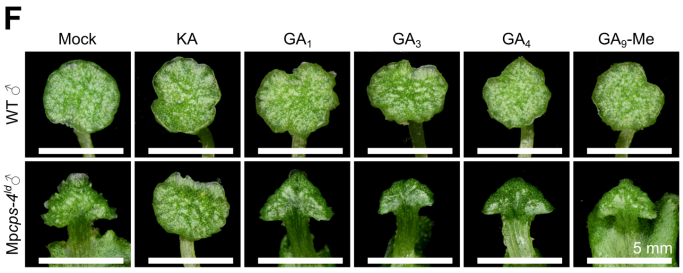

Figure 3 Endogenous levels of and responsiveness to KA or GAs in wild-type and Mp*cps*^{ld} plants.
A, Endogenous levels of GAs measured in wild-type plants (Tak-1) by LC-MS/MS. B, Selected ion chromatography showing peak of endogenous GA_{12} in comparison with the $^{2}H_{2}$-labeled internal standard. For A-B, plants were cultured under cW for 10 days, then induced under cW+cFR for 3 days. C-D, Effect of 2-μM KA or GAs on the morphology of 12-day-old thalli cultured under cW+cFR from gemmae. Horizontal bars in D represent mean values, and letters represent multiple comparisons with non-pooled Welch's *t*-test and B-H adjustment (adjusted $p<0.05$ for non-overlapping letters, n=16-18). E-F, Effect of 2-μM KA or GAs on gametangiophore formation (E) and morphology (F). Plants were cultured aseptically under cW for 7 days before transferred to cW+cFR. Dots and error bars represent mean±SD in E (n=5). Bars = 10 mm in C and 5 mm in F.

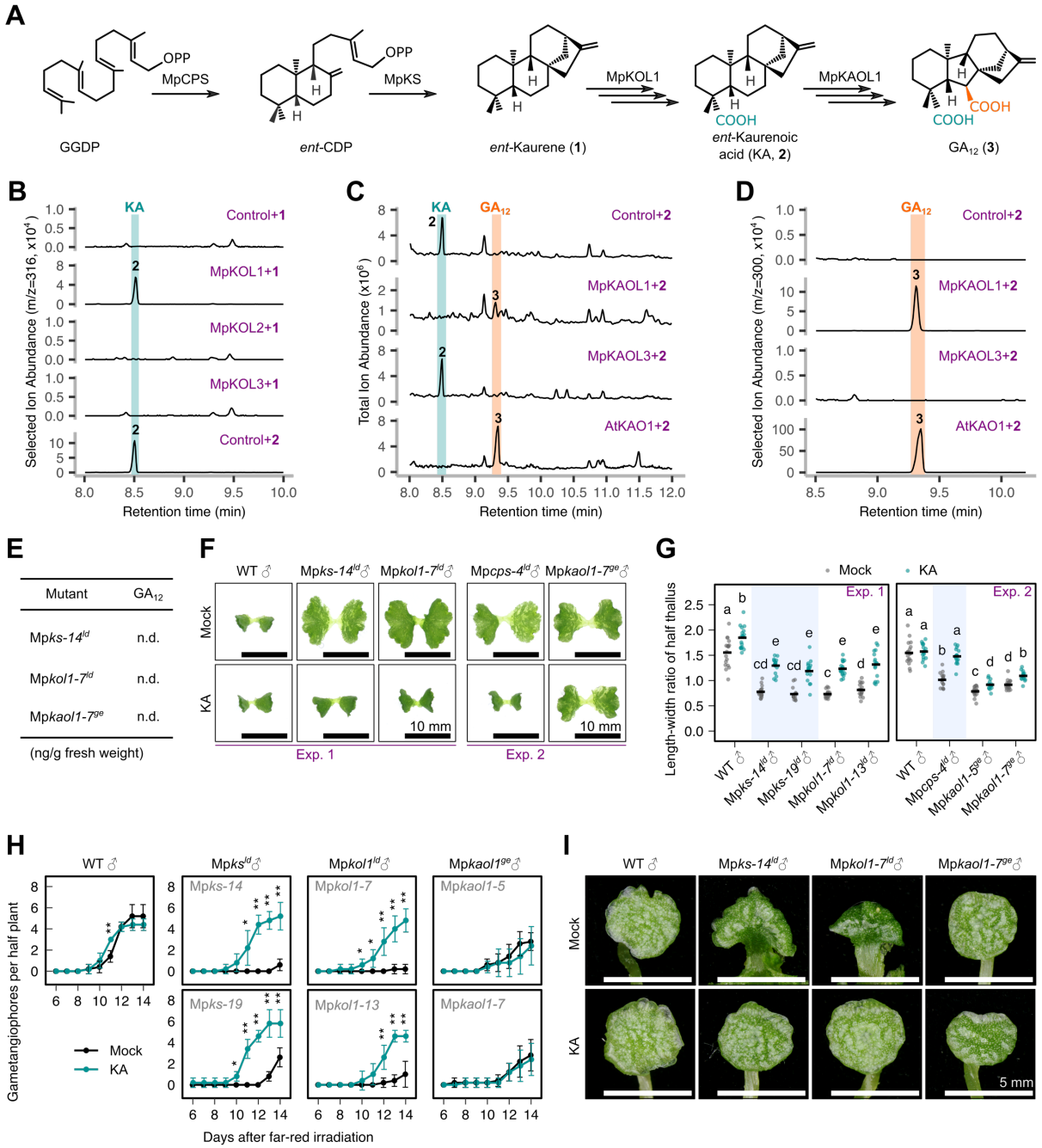
A
OPP
MpCPS
OPP
MpKS
MpKOL1
MpKAOL1
COOH
COOH
COOH
GGDP
ent-CDP
ent-Kaurene (1)
ent-Kaurenoic acid (KA, 2)
GA12 (3)
B
KA
Control+1
MpKOL1+1
MpKOL2+1
MpKOL3+1
Control+2
Selected Ion Abundance (m/z=316, x10^4)
Retention time (min)
C
KA
GA12
Control+2
MpKAOL1+2
MpKAOL3+2
AtKAO1+2
Total Ion Abundance (x10^6)
Retention time (min)
D
GA12
Control+2
MpKAOL1+2
MpKAOL3+2
AtKAO1+2
Selected Ion Abundance (m/z=300, x10^4)
Retention time (min)
E
Mutant
GA12
Mpks-14ld
n.d.
Mpkol1-7ld
n.d.
Mpkaol1-7ge
n.d.
(ng/g fresh weight)
F
WT ♂
Mpks-14ld♂
Mpkol1-7ld♂
Mpcps-4ld♂
Mpkaol1-7ge♂
Mock
KA
10 mm
10 mm
Exp. 1
Exp. 2
G
Mock
KA
Exp. 1
Exp. 2
Length-width ratio of half thallus
WT ♂
Mpks-14ld♂
Mpks-19ld♂
Mpkol1-7ld♂
Mpkol1-13ld♂
WT ♂
Mpcps-4ld♂
Mpkaol1-5ge♂
Mpkaol1-7ge♂
H
WT ♂
Mpksld♂
Mpkol1ld♂
Mpkaol1ge♂
Mpks-14
Mpks-19
Mpkol1-7
Mpkol1-13
Mpkaol1-5
Mpkaol1-7
Gametangiophores per half plant
Mock
KA
Days after far-red irradiation
I
WT ♂
Mpks-14ld♂
Mpkol1-7ld♂
Mpkaol1-7ge♂
Mock
KA
5 mm

Figure 4 Biosynthetic route for GA_{12} production in *M. polymorpha*.
A, Proposed enzymatic steps for GA_{12} biosynthesis in *M. poymorpha*. B-D, GC-MS analysis showing conversion of *ent*-kaurene to KA (B), and KA to GA_{12} (C-D) by yeast cultures expressing KO and KAO homologs. E, biosynthesis mutants with GA_{12} below the detection limit. n.d., not detected. F-G, morphlogy of 12-day-old mutants grown under cW+cFR with or without 2 μM KA. Horizontal bars in G represent mean values, and letters represent multiple comparisons with non-pooled Welch's *t*-test and B-H adjustment (adjusted $p<0.05$ for non-overlapping letters, n=14-18). H-I, Gametangiophore formation progress (H) and morphology (I) of mutants, cultured aseptically under cW for 7 days before transferred to cW+cFR and treated with 2 μM KA. Dots and error bars represent mean±SD in H (n=5). Bars = 10 mm in F and 5 mm in I.

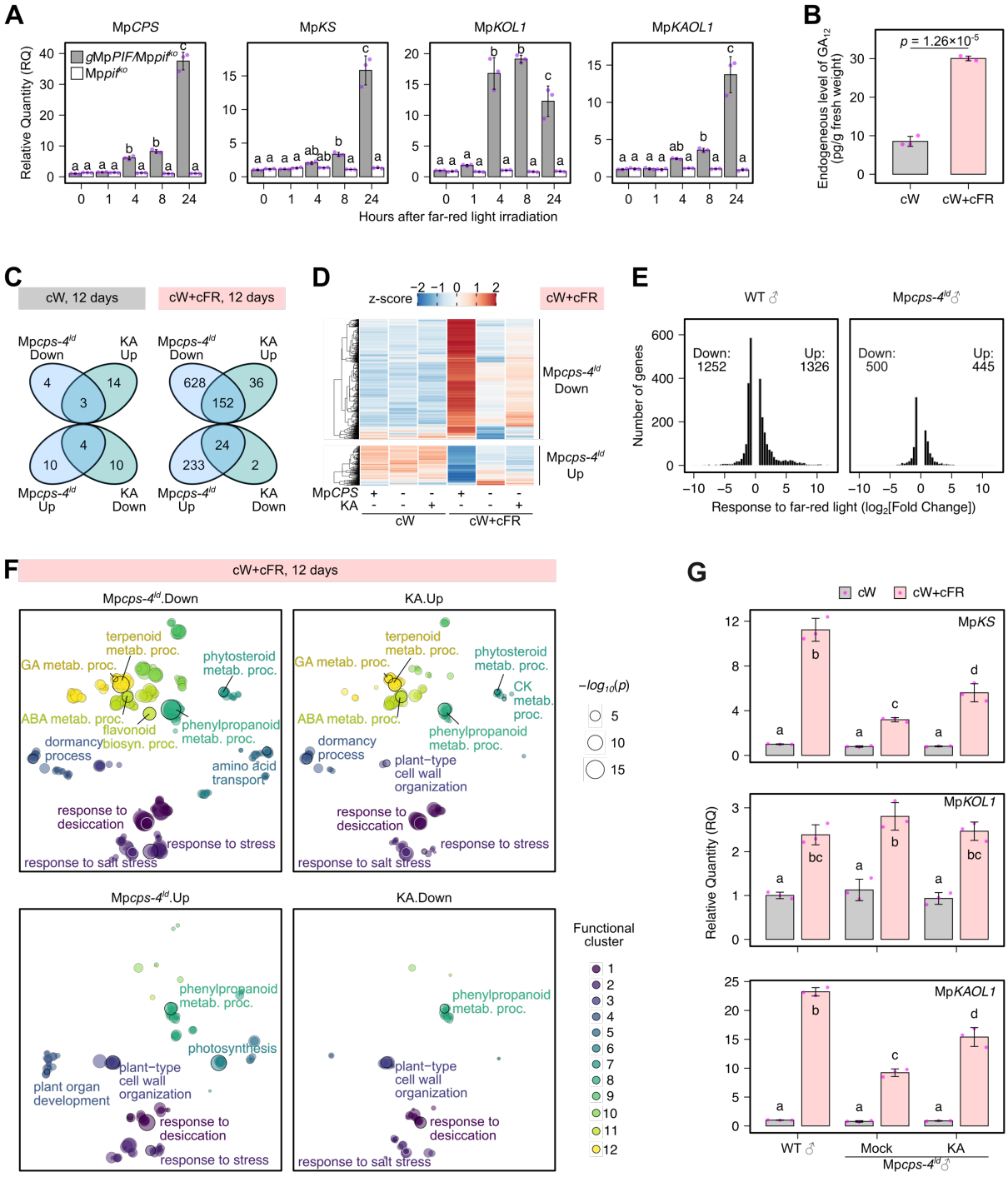
A
MpCPS
MpKS
MpKOL1
MpKAOL1
Relative Quantity (RQ)
gMpPIF/Mppif^ko
Mppif^ko
Hours after far-red light irradiation
B
Endogeneous level of GA12 (pg/g fresh weight)
p = 1.26×10^-5
cW
cW+cFR
C
cW, 12 days
cW+cFR, 12 days
Mpcps-4^ld Down
KA Up
Mpcps-4^ld Up
KA Down
D
z-score
cW+cFR
Mpcps-4^ld Down
Mpcps-4^ld Up
MpCPS
KA
cW
cW+cFR
E
WT ♂
Mpcps-4^ld ♂
Number of genes
Down: 1252
Up: 1326
Down: 500
Up: 445
Response to far-red light (log2[Fold Change])
F
cW+cFR, 12 days
Mpcps-4^ld.Down
KA.Up
Mpcps-4^ld.Up
KA.Down
terpenoid metab. proc.
phytosteroid metab. proc.
GA metab. proc.
ABA metab. proc.
flavonoid biosyn. proc.
phenylpropanoid metab. proc.
dormancy process
amino acid transport
CK metab. proc.
plant-type cell wall organization
response to desiccation
response to stress
response to salt stress
photosynthesis
plant organ development
−log10(p)
Functional cluster
G
cW
cW+cFR
MpKS
MpKOL1
MpKAOL1
Relative Quantity (RQ)
WT ♂
Mock
KA
Mpcps-4^ld ♂

Figure 5 Transcriptional regulation related to GA biosynthesis in *M. polymorpha*.
A, Relative expression level of GA biosynthesis genes by qPCR in Mp*pif*^{ko} and its complementation line, cultured under cW for 7 days and then transferred to cW+cFR. B, endogenous level of GA_{12} in Tak-1 plants cultured under cW for 10 days, then under cW or cW+cFR for 4 days. The data for cW+cFR group is the same as in Figure 3A. The *p*-value was calculated by Student's *t*-test. C, Number of differentially expressed genes (DEGs) between 12-day-old Mp*cps*^{ld} and Tak-1 plants, or Mp*cps-4*^{ld} plants grown with or without 2-μM KA under indicated light conditions (Wald test with B-H adjustment by DESeq2, DEG defined as adjusted $p<0.01$ and $|\log_2(\text{Fold Change})|>0.585$). D, expression patterns of up- and down-regulated genes in Mp*cps-4*^{ld}. E, Distribution of DEGs induced by FR enrichment in Tak-1 and Mp*cps-4*^{ld} plants, comparing transcriptomes of cW+cFR to cW conditions. F, GO term enrichment analysis of DEG sets shown in (C). Each dot shows a significant enriched biological process term ($p<0.01$ by Fisher's exact test), and semantically similar terms were plotted in color-coded clusters. Selected terms were highlighted with annotations. metab. proc., metabolic process. See Supplemental Data Set 2 for full lists. G, Relative expression level of GA biosynthesis genes by qPCR in plants cultured under cW for 11 days, then transferred to cW+cFR with or without 2-μM KA treatment. All bar plots with error bars (A-B, G) represent mean±SD from 3 biological replicates. Letters in A and G represent multiple comparisons with Tukey's HSD test (adjusted $p<0.05$ for non-overlapping letters).

Parsed Citations

Achard, P., Gusti, A., Cheminant, S., Alioua, M., Dhondt, S., Coppens, F., Beemster, G.T.S., and Genschik, P. (2009). Gibberellin Signaling Controls Cell Proliferation Rate in Arabidopsis. Current Biology 19: 1188–1193.
Google Scholar: Author Only Title Only Author and Title

Aki, S.S., Mikami, T., Naramoto, S., Nishihama, R., Ishizaki, K., Kojima, M., Takebayashi, Y., Sakakibara, H., Kyozuka, J., Kohchi, T., and Umeda, M. (2019). Cytokinin Signaling Is Essential for Organ Formation in Marchantia polymorpha. Plant and Cell Physiology 60: 1842–1854.
Google Scholar: Author Only Title Only Author and Title

Alexa, A. and Rahnenfuhrer, J. (2022). topGO: Enrichment Analysis for Gene Ontology. R package version 2.50.0.
Google Scholar: Author Only Title Only Author and Title

Althoff, F., Kopischke, S., Zobell, O., Ide, K., Ishizaki, K., Kohchi, T., and Zachgo, S. (2014). Comparison of the MpEF1α and CaMV35 promoters for application in Marchantia polymorpha overexpression studies. Transgenic Res 23: 235–244.
Google Scholar: Author Only Title Only Author and Title

Altschul, S.F., Gish, W., Miller, W., Myers, E.W., and Lipman, D.J. (1990). Basic local alignment search tool. Journal of Molecular Biology 215: 403–410.
Google Scholar: Author Only Title Only Author and Title

Beall, F.D., Yeung, E.C., and Pharis, R.P. (1996). Far-red light stimulates internode elongation, cell division, cell elongation, and gibberellin levels in bean. Can. J. Bot. 74: 743–752.
Google Scholar: Author Only Title Only Author and Title

Bou-Torrent, J., Galstyan, A., Gallemí, M., Cifuentes-Esquivel, N., Molina-Contreras, M.J., Salla-Martret, M., Jikumaru, Y., Yamaguchi, S., Kamiya, Y., and Martínez-García, J.F. (2014). Plant proximity perception dynamically modulates hormone levels and sensitivity in Arabidopsis. Journal of Experimental Botany 65: 2937–2947.
Google Scholar: Author Only Title Only Author and Title

Bowman, J.L. et al. (2017). Insights into land plant evolution garnered from the Marchantia polymorpha genome. Cell 171: 287-304.e15.
Google Scholar: Author Only Title Only Author and Title

Briginshaw, L.N., Flores-Sandoval, E., Dierschke, T., Alvarez, J.P., and Bowman, J.L. (2022). KANADI promotes thallus differentiation and FR-induced gametangiophore formation in the liverwort Marchantia. New Phytologist 234: 1377–1393.
Google Scholar: Author Only Title Only Author and Title

Cannell, N., Emms, D.M., Hetherington, A.J., MacKay, J., Kelly, S., Dolan, L., and Sweetlove, L.J. (2020). Multiple Metabolic Innovations and Losses Are Associated with Major Transitions in Land Plant Evolution. Current Biology 30: 1783-1800.e11.
Google Scholar: Author Only Title Only Author and Title

Cao, J.-G., Wang, Q.-X., Zou, H.-M., Dai, X.-L., and Cao, T. (2013). New Observations on the Morphology and Structure of Marchantia polymorpha Gametophores in Sexual Reproduction Adaption. Plant Science Journal 31: 555.
Google Scholar: Author Only Title Only Author and Title

Chiang, H.-H., Hwang, I., and Goodman, H.M. (1995). Isolation of the Arabidopsis GA4 locus. the Plant Cell 7: 195–201.
Google Scholar: Author Only Title Only Author and Title

Chiyoda, S., Ishizaki, K., Kataoka, H., Yamato, K.T., and Kohchi, T. (2008). Direct transformation of the liverwort Marchantia polymorpha L. by particle bombardment using immature thalli developing from spores. Plant Cell Reports 27: 1467–1473.
Google Scholar: Author Only Title Only Author and Title

Conesa, A. and Götz, S. (2008). Blast2GO: A comprehensive suite for functional analysis in plant genomics. International Journal of Plant Genomics 2008.
Google Scholar: Author Only Title Only Author and Title

Djakovic-Petrovic, T., Wit, M.D., Voesenek, L.A.C.J., and Pierik, R. (2007). DELLA protein function in growth responses to canopy signals. Plant Journal 51: 117–126.
Google Scholar: Author Only Title Only Author and Title

Downs, R.J., Hendricks, S.B., and Borthwick, H.A. (1957). Photoreversible Control of Elongation of Pinto Beans and Other Plants under Normal Conditions of Growth. Botanical Gazette 118: 199–208.
Google Scholar: Author Only Title Only Author and Title

Dubois, P.G., Olsefski, G.T., Flint-Garcia, S., Setter, T.L., Hoekenga, O.A., and Brutnell, T.P. (2010). Physiological and Genetic Characterization of End-of-Day Far-Red Light Response in Maize Seedlings. Plant Physiology 154: 173–186.
Google Scholar: Author Only Title Only Author and Title

Fredericq, H. (1964). Influence formatrice de la lumière rouge-foncé sur le développement des thalles de Marchantia polymorpha L. Bull. Soc. Roy. Bot. Belgique 98: 67–76.
Google Scholar: Author Only Title Only Author and Title

Fredericq, H. and de Greef, J. (1966). Red (R), Far-red (FR) photoreversible control of growth and chlorophyll content in light-grown thalli of Marchantia polymorpha L. Die Naturwissenschaften 53: 337.
Google Scholar: Author Only Title Only Author and Title

Fredericq, H. and Greef, J.D. (1968). Photomorphogenic and Chlorophyll Studies in the Bryophyte Marchantia polymorpha. I. Effect of Red, Far-red Irradiations in Short and Long-term Experiments. Physiol Plant 21: 346–359.
Google Scholar: Author Only Title Only Author and Title

Gabriele, S., Rizza, A., Martone, J., Circelli, P., Costantino, P., and Vittorioso, P. (2009). The Dof protein DAG1 mediates PIL5 activity on seed germination by negatively regulating GA biosynthetic gene AtGA3ox1: DAG1 represses seed germination via PIL5 signalling. The Plant Journal 61: 312–323.
Google Scholar: Author Only Title Only Author and Title

Gamborg, O.L., Miller, R.A., and Ojima, K. (1968). Nutrient requirements of suspension cultures of soybean root cells. Experimental Cell Research 50: 151–158.
Google Scholar: Author Only Title Only Author and Title

García-Martínez, J.L., Keith, B., Bonner, B.A., Stafford, A.E., and Rappaport, L. (1987). Phytochrome Regulation of the Response to Exogenous Gibberellins by Epicotyls of Vigna sinensis. Plant Physiol. 85: 212–216.
Google Scholar: Author Only Title Only Author and Title

Guindon, S., Dufayard, J.-F., Lefort, V., Anisimova, M., Hordijk, W., and Gascuel, O. (2010). New algorithms and methods to estimate maximum-likelihood phylogenies: Assessing the performance of PhyML 3.0. Systematic Biology 59: 307–321.
Google Scholar: Author Only Title Only Author and Title

Hayashi, K., Horie, K., Hiwatashi, Y., Kawaide, H., Yamaguchi, S., Hanada, A., Nakashima, T., Nakajima, M., Mander, L.N., Yamane, H., Hasebe, M., and Nozaki, H. (2010). Endogenous diterpenes derived from ent-kaurene, a common gibberellin precursor, regulate protonema differentiation of the moss Physcomitrella patens. Plant Physiology 153: 1085–1097.
Google Scholar: Author Only Title Only Author and Title

Hayashi, K. ichiro, Kawaide, H., Notomi, M., Sakigi, Y., Matsuo, A., and Nozaki, H. (2006). Identification and functional analysis of bifunctional ent-kaurene synthase from the moss Physcomitrella patens. FEBS Letters 580: 6175–6181.
Google Scholar: Author Only Title Only Author and Title

Hedden, P. (2020). The Current Status of Research on Gibberellin Biosynthesis. Plant and Cell Physiology 61: 1832–1849.
Google Scholar: Author Only Title Only Author and Title

Hedden, P., MacMillan, J., and Phinney, B.O. (1974). Fungal products. Part XII. Gibberellin A14-aldehyde, an intermediate in gibberellin biosynthesis in Gibberella fujikuroi. Journal of the Chemical Society, Perkin Transactions 1: 587–592.
Google Scholar: Author Only Title Only Author and Title

Hellemans, J., Mortier, G., De Paepe, A., Speleman, F., and Vandesompele, J. (2008). qBase relative quantification framework and software for management and automated analysis of real-time quantitative PCR data. Genome Biology 8.
Google Scholar: Author Only Title Only Author and Title

Helliwell, C.A., Chandler, P.M., Poole, A., Dennis, E.S., and Peacock, W.J. (2001a). The CYP88A cytochrome P450, ent-kaurenoic acid oxidase, catalyzes three steps of the gibberellin biosynthesis pathway. Proceedings of the National Academy of Sciences of the United States of America 98: 2065–2070.
Google Scholar: Author Only Title Only Author and Title

Helliwell, C.A., Poole, A., James Peacock, W., and Dennis, E.S. (1999). Arabidopsis ent -kaurene oxidase catalyzes three steps of gibberellin biosynthesis. Plant Physiology 119: 507–510.
Google Scholar: Author Only Title Only Author and Title

Helliwell, C.A., Sheldon, C.C., Olive, M.R., R.Walker, A., Zeevaart, J.A.D., Peacock, W.J., and Dennis, E.S. (1998). Cloning of the Arabidopsis ent-kaurene oxidase gene GA3. Proceedings of the National Academy of Sciences of the United States of America 95: 9019–9024.
Google Scholar: Author Only Title Only Author and Title

Helliwell, C.A., Sullivan, J.A., Mould, R.M., Gray, J.C., James Peacock, W., and Dennis, E.S. (2001b). A plastid envelope location of Arabidopsis ent-kaurene oxidase links the plastid and endoplasmic reticulum steps of the gibberellin biosynthesis pathway. Plant Journal 28: 201–208.
Google Scholar: Author Only Title Only Author and Title

Hernández-García, J., Sun, R., Serrano-Mislata, A., Inoue, K., Vargas-Chávez, C., Esteve-Bruna, D., Arbona, V., Yamaoka, S., Nishihama, R., Kohchi, T., and Blázquez, M.A. (2021). Coordination between growth and stress responses by DELLA in the

liverwort Marchantia polymorpha. Current Biology.
Google Scholar: Author Only Title Only Author and Title

Hirano, K. et al. (2007). The GID1-mediated gibberellin perception mechanism is conserved in the lycophyte Selaginella moellendorffii but not in the bryophyte Physcomitrella patens. The Plant Cell 19: 3058–3079.
Google Scholar: Author Only Title Only Author and Title

Hisamatsu, T., King, R.W., Helliwell, C. a, and Koshioka, M. (2005). The involvement of gibberellin 20-oxidase genes in phytochrome-regulated petiole elongation of Arabidopsis. Plant Physiology 138: 1106–1116.
Google Scholar: Author Only Title Only Author and Title

Hisanaga, T., Okahashi, K., Yamaoka, S., Kajiwara, T., Nishihama, R., Shimamura, M., Yamato, K.T., Bowman, J.L., Kohchi, T., and Nakajima, K. (2019). A cis -acting bidirectional transcription switch controls sexual dimorphism in the liverwort. The EMBO Journal 38: 1–12.
Google Scholar: Author Only Title Only Author and Title

Hoang, D.T., Chernomor, O., von Haeseler, A., Minh, B.Q., and Vinh, L.S. (2018). UFBoot2: Improving the Ultrafast Bootstrap Approximation. Molecular Biology and Evolution 35: 518–522.
Google Scholar: Author Only Title Only Author and Title

Holmes, M.G. and Smith, H. (1975). The function of phytochrome in plants growing in the natural environment. Nature 254: 512–514.
Google Scholar: Author Only Title Only Author and Title

Hornych, O., Testo, W.L., Sessa, E.B., Watkins, J.E., Campany, C.E., Pittermann, J., and Ekrt, L. (2021). Insights into the evolutionary history and widespread occurrence of antheridiogen systems in ferns. New Phytologist 229: 607–619.
Google Scholar: Author Only Title Only Author and Title

Inoue, K., Nishihama, R., Araki, T., and Kohchi, T. (2019). Reproductive induction is a far-red high irradiance response that is mediated by phytochrome and PHYTOCHROME INTERACTING FACTOR in Marchantia polymorpha. Plant and Cell Physiology 60: 1136–1145.
Google Scholar: Author Only Title Only Author and Title

Inoue, K., Nishihama, R., Kataoka, H., Hosaka, M., Manabe, R., Nomoto, M., Tada, Y., Ishizaki, K., and Kohchi, T. (2016). Phytochrome signaling is mediated by PHYTOCHROME INTERACTING FACTOR in the liverwort Marchantia polymorpha. The Plant Cell 28: 1406–1421.
Google Scholar: Author Only Title Only Author and Title

Ishizaki, K., Chiyoda, S., Yamato, K.T., and Kohchi, T. (2008). Agrobacterium-mediated transformation of the haploid liverwort Marchantia polymorpha L., an emerging model for plant biology. Plant and Cell Physiology 49: 1084–1091.
Google Scholar: Author Only Title Only Author and Title

Ishizaki, K., Nishihama, R., Ueda, M., Inoue, K., Ishida, S., Nishimura, Y., Shikanai, T., and Kohchi, T. (2015). Development of Gateway binary vector series with four different selection markers for the liverwort Marchantia polymorpha. PLoS ONE 10: e0138876.
Google Scholar: Author Only Title Only Author and Title

Iwasaki, M. et al. (2021). Identification of the sex-determining factor in the liverwort Marchantia polymorpha reveals unique evolution of sex chromosomes in a haploid system. Current Biology 31: 5522-5532.e7.
Google Scholar: Author Only Title Only Author and Title

Jia, Q., Brown, R., Köllner, T.G., Fu, J., Chen, X., Wong, G.K.S., Gershenzon, J., Peters, R.J., and Chen, F. (2022). Origin and early evolution of the plant terpene synthase family. Proceedings of the National Academy of Sciences of the United States of America 119: 1–9.
Google Scholar: Author Only Title Only Author and Title

Kalyaanamoorthy, S., Minh, B.Q., Wong, T.K.F., von Haeseler, A., and Jermiin, L.S. (2017). ModelFinder: fast model selection for accurate phylogenetic estimates. Nat Methods 14: 587–589.
Google Scholar: Author Only Title Only Author and Title

Katoh, K. and Standley, D.M. (2013). MAFFT multiple sequence alignment software version 7: Improvements in performance and usability. Molecular Biology and Evolution 30: 772–780.
Google Scholar: Author Only Title Only Author and Title

Katsumata, T., Hasegawa, A., Fujiwara, T., Komatsu, T., Notomi, M., Abe, H., Natsume, M., and Kawaide, H. (2008). Arabidopsis CYP85A2 Catalyzes Lactonization Reactions in the Biosynthesis of 2-Deoxy-7-oxalactone Brassinosteroids. Bioscience, Biotechnology, and Biochemistry 72: 2110–2117.
Google Scholar: Author Only Title Only Author and Title

Kohnen, M.V., Schmid-Siegert, E., Trevisan, M., Petrolati, L.A., Sénéchal, F., Müller-Moulé, P., Maloof, J., Xenarios, I., and

Fankhauser, C. (2016). Neighbor Detection Induces Organ-Specific Transcriptomes, Revealing Patterns Underlying Hypocotyl-Specific Growth. Plant Cell 28: 2889–2904.
Google Scholar: Author Only Title Only Author and Title

Koide, E., Suetsugu, N., Iwano, M., Gotoh, E., Nomura, Y., Stolze, S.C., Nakagami, H., Kohchi, T., and Nishihama, R. (2020). Regulation of Photosynthetic Carbohydrate Metabolism by a Raf-Like Kinase in the Liverwort Marchantia polymorpha. Plant and Cell Physiology 61: 631–643.
Google Scholar: Author Only Title Only Author and Title

Koornneef, M. and van der Veen, J.H. (1980). Induction and analysis of gibberellin sensitive mutants in Arabidopsis thaliana (L.) heynh. Theoretical and Applied Genetics 58: 257–263.
Google Scholar: Author Only Title Only Author and Title

Krijthe, J.H. (2015). Rtsne: T-Distributed Stochastic Neighbor Embedding using a Barnes-Hut Implementation.

Kubota, A., Ishizaki, K., Hosaka, M., and Kohchi, T. (2013). Efficient Agrobacterium-mediated transformation of the liverwort Marchantia polymorpha using regenerating thalli. Bioscience, Biotechnology and Biochemistry 77: 167–172.
Google Scholar: Author Only Title Only Author and Title

Kumar, S. et al. (2016). Molecular diversity of terpene synthases in the liverwort Marchantia polymorpha. The Plant Cell 28: 2632–2650.
Google Scholar: Author Only Title Only Author and Title

Küpers, J.J. et al. (2023). Local light signaling at the leaf tip drives remote differential petiole growth through auxin-gibberellin dynamics. Current Biology 33: 75-85.e5.
Google Scholar: Author Only Title Only Author and Title

Kurihara, D., Mizuta, Y., Nagahara, S., and Higashiyama, T. (2021). ClearSeeAlpha: Advanced Optical Clearing for Whole-Plant Imaging. Plant and Cell Physiology 62: 1302–1310.
Google Scholar: Author Only Title Only Author and Title

Kurosawa, E. (1926). Experimental studies on the nature of the substance excreted by the "bakanae" fungus. Trans. Nat. Hist. Soc. Formosa 16: 213–227.
Google Scholar: Author Only Title Only Author and Title

Li, W., Liu, S.-W., Ma, J.-J., Liu, H.-M., Han, F.-X., Li, Y., and Niu, S.-H. (2020). Gibberellin Signaling Is Required for Far-Red Light-Induced Shoot Elongation in Pinus tabuliformis Seedlings. Plant Physiol. 182: 658–668.
Google Scholar: Author Only Title Only Author and Title

Love, M.I., Huber, W., and Anders, S. (2014). Moderated estimation of fold change and dispersion for RNA-seq data with DESeq2. Genome Biology 15: 550.
Google Scholar: Author Only Title Only Author and Title

Michaud, O., Krahmer, J., Galbier, F., Lagier, M., Galvão, V.C., Ince, Y.Ç., Trevisan, M., Knerova, J., Dickinson, P., Hibberd, J.M., Zeeman, S.C., and Fankhauser, C. (2023). Abscisic acid modulates neighbor proximity-induced leaf hyponasty in Arabidopsis. Plant Physiology 191: 542–557.
Google Scholar: Author Only Title Only Author and Title

Minh, B.Q., Schmidt, H.A., Chernomor, O., Schrempf, D., Woodhams, M.D., von Haeseler, A., and Lanfear, R. (2020). IQ-TREE 2: New Models and Efficient Methods for Phylogenetic Inference in the Genomic Era. Molecular Biology and Evolution 37: 1530–1534.
Google Scholar: Author Only Title Only Author and Title

Miyazaki, S., Hara, M., Ito, S., Tanaka, K., Asami, T., Hayashi, K., Kawaide, H., and Nakajima, M. (2018). An Ancestral Gibberellin in a Moss Physcomitrella patens. Molecular Plant 11: 1097–1100.
Google Scholar: Author Only Title Only Author and Title

Miyazaki, S., Katsumata, T., Natsume, M., and Kawaide, H. (2011). The CYP701B1 of Physcomitrella patens is an ent-kaurene oxidase that resists inhibition by uniconazole-P. FEBS Letters 585: 1879–1883.
Google Scholar: Author Only Title Only Author and Title

Miyazaki, S., Nakajima, M., and Kawaide, H. (2015). Hormonal diterpenoids derived from ent-kaurenoic acid are involved in the blue-light avoidance response of Physcomitrella patens. Plant Signaling and Behavior 10: 1–4.
Google Scholar: Author Only Title Only Author and Title

Miyazaki, S., Toyoshima, H., Natsume, M., Nakajima, M., and Kawaide, H. (2014). Blue-light irradiation up-regulates the ent-kaurene synthase gene and affects the avoidance response of protonemal growth in Physcomitrella patens. Planta 240: 117–124.
Google Scholar: Author Only Title Only Author and Title

Morgan, D.C. and Smith, H. (1979). A systematic relationship between phytochrome-controlled development and species habitat,

for plants grown in simulated natural radiation. Planta 145: 253–258.
Google Scholar: Author Only Title Only Author and Title

Morgan, D.C. and Smith, H. (1978). The relationship between phytochrome-photoequilibrium and Development in light grown Chenopodium album L. Planta 142: 187–193.
Google Scholar: Author Only Title Only Author and Title

Motohashi, K. (2015). A simple and efficient seamless DNA cloning method using SLiCE from Escherichia coli laboratory strains and its application to SLiP site-directed mutagenesis. BMC Biotechnol 15: 47.
Google Scholar: Author Only Title Only Author and Title

Näf, U., Nakanishi, K., and Endo, M. (1975). On the Physiology and Chemistry of Fern Antheridiogens. Botanical Review 41: 315–359.
Google Scholar: Author Only Title Only Author and Title

Nelissen, H., Rymen, B., Jikumaru, Y., Demuynck, K., Van Lijsebettens, M., Kamiya, Y., Inzé, D., and Beemster, G.T.S. (2012). A Local Maximum in Gibberellin Levels Regulates Maize Leaf Growth by Spatial Control of Cell Division. Current Biology 22: 1183–1187.
Google Scholar: Author Only Title Only Author and Title

Ninnemann, H. and Halbsguth, W. (1965). Rolle des Phytochroms beim Etiolement von Marchantia polymorpha. Naturwissenschaften 52: 110–111.
Google Scholar: Author Only Title Only Author and Title

Nomura, T., Magome, H., Hanada, A., Takeda-Kamiya, N., Mander, L.N., Kamiya, Y., and Yamaguchi, S. (2013). Functional analysis of Arabidopsis CYP714A1 and CYP714A2 reveals that they are distinct gibberellin modification enzymes. Plant and Cell Physiology 54: 1837–1851.
Google Scholar: Author Only Title Only Author and Title

Ogawa, M., Hanada, A., Yamauchi, Y., Kuwahara, A., Kamiya, Y., and Yamaguchi, S. (2003). Gibberellin Biosynthesis and Response during Arabidopsis Seed Germination. The Plant Cell 15: 1591–1604.
Google Scholar: Author Only Title Only Author and Title

Patro, R., Duggal, G., Love, M.I., Irizarry, R.A., and Kingsford, C. (2017). Salmon provides fast and bias-aware quantification of transcript expression. Nature Methods 14: 417–419.
Google Scholar: Author Only Title Only Author and Title

Pluthero, F.G. (1993). Rapid purification of high-activity Taq DNA polymerase. Nucleic Acids Res 21: 4850–4851.
Google Scholar: Author Only Title Only Author and Title

Rojas, M.C., Hedden, P., Gaskin, P., and Tudzynski, B. (2001). The P450–1 gene of Gibberella fujikuroi encodes a multifunctional enzyme in gibberellin biosynthesis. Proc. Natl. Acad. Sci. U.S.A. 98: 5838–5843.
Google Scholar: Author Only Title Only Author and Title

Sakamoto, Y., Ishimoto, A., Sakai, Y., Sato, M., Nishihama, R., Abe, K., Sano, Y., Furuichi, T., Tsuji, H., Kohchi, T., and Matsunaga, S. (2022). Improved clearing method contributes to deep imaging of plant organs. Commun Biol 5: 12.
Google Scholar: Author Only Title Only Author and Title

Schindelin, J. et al. (2012). Fiji: an open-source platform for biological-image analysis. Nat Methods 9: 676–682.
Google Scholar: Author Only Title Only Author and Title

Schmidt, U., Weigert, M., Broaddus, C., and Myers, G. (2018). Cell Detection with Star-Convex Polygons. In Medical Image Computing and Computer Assisted Intervention – MICCAI 2018, A.F. Frangi, J.A. Schnabel, C. Davatzikos, C. Alberola-López, and G. Fichtinger, eds, Lecture Notes in Computer Science. (Springer International Publishing: Cham), pp. 265–273.
Google Scholar: Author Only Title Only Author and Title

Schneller, J.J. (2008). Antheridiogens. In Biology and Evolution of Ferns and Lycophytes, T.A. Ranker and C.H. Haufler, eds (Cambridge University Press: New York), pp. 134–158.
Google Scholar: Author Only Title Only Author and Title

Sessa, G., Carabelli, M., Sassi, M., Ciolfi, A., Possenti, M., Mittempergher, F., Becker, J., Morelli, G., and Ruberti, I. (2005). A dynamic balance between gene activation and repression regulates the shade avoidance response in Arabidopsis. Genes Dev. 19: 2811–2815.
Google Scholar: Author Only Title Only Author and Title

Shimamura, M. (2016). Marchantia polymorpha: Taxonomy, phylogeny and morphology of a model system. Plant and Cell Physiology 57: 230–256.
Google Scholar: Author Only Title Only Author and Title

Sponsel, V.M. (2016). Signal achievements in gibberellin research: the second half-century. Annual Plant Reviews: The

Gibberellins 49: 1–36.
Google Scholar: Author Only Title Only Author and Title

Streubel, S., Deiber, S., Rötzer, J., Mosiolek, M., Jandrasits, K., and Dolan, L. (2023). Meristem dormancy in Marchantia polymorpha is regulated by a liverwort-specific miRNA and a clade III SPL gene. Current Biology: S0960982222019996.
Google Scholar: Author Only Title Only Author and Title

Sugano, S.S., Nishihama, R., Shirakawa, M., Takagi, J., Matsuda, Y., Ishida, S., Shimada, T., Hara-Nishimura, I., Osakabe, K., and Kohchi, T. (2018). Efficient CRISPR/Cas9-based genome editing and its application to conditional genetic analysis in Marchantia polymorpha. PLoS ONE 13: e0205117.
Google Scholar: Author Only Title Only Author and Title

Sun, T. and Kamiya, Y. (1994). The Arabidopsis GA1 locus encodes the cyclase ent-kaurene synthetase A of gibberellin biosynthesis. the Plant Cell 6: 1509–1518.
Google Scholar: Author Only Title Only Author and Title

Talon, M., Koornneef, M., and Zeevaart, J.A.D. (1990). Endogenous gibberellins in Arabidopsis thaliana and possible steps blocked in the biosynthetic pathways of the semidwarf ga4 and ga5 mutants. Proceedings of the National Academy of Sciences of the United States of America 87: 7983–7987.
Google Scholar: Author Only Title Only Author and Title

Tanaka, J., Yano, K., Aya, K., Hirano, K., Takehara, S., Koketsu, E., Ordonio, R.L., Park, S.-H., Nakajima, M., Ueguchi-Tanaka, M., and Matsuoka, M. (2014). Antheridiogen determines sex in ferns via a spatiotemporally split gibberellin synthesis pathway. Science 346: 469–473.
Google Scholar: Author Only Title Only Author and Title

Toyomasu, T., Kawaide, H., Mitsuhashi, W., Inoue, Y., and Kamiya, Y. (1998). Phytochrome regulates gibberellin biosynthesis during germination of photoblastic lettuce seeds. Plant Physiology 118: 1517–1523.
Google Scholar: Author Only Title Only Author and Title

Ubeda-Tomás, S., Federici, F., Casimiro, I., Beemster, G.T.S., Bhalerao, R., Swarup, R., Doerner, P., Haseloff, J., and Bennett, M.J. (2009). Gibberellin Signaling in the Endodermis Controls Arabidopsis Root Meristem Size. Current Biology 19: 1194–1199.
Google Scholar: Author Only Title Only Author and Title

Ubeda-Tomás, S., Swarup, R., Coates, J., Swarup, K., Laplaze, L., Beemster, G.T.S., Hedden, P., Bhalerao, R., and Bennett, M.J. (2008). Root growth in Arabidopsis requires gibberellin/DELLA signalling in the endodermis. Nat Cell Biol 10: 625–628.
Google Scholar: Author Only Title Only Author and Title

Urrutia, O., Hedden, P., and Rojas, M.C. (2001). Monooxygenases involved in GA12 and GA14 synthesis in Gibberella fujikuroi. Phytochemistry 56: 505–511.
Google Scholar: Author Only Title Only Author and Title

Van Tuinen, A., Peters, A.H.L.J., Kendrick, R.E., Zeevaart, J. a. D., and Koornneef, M. (1999). Characterisation of the procera mutant of tomato and the interaction of gibberellins with end-of-day far-red light treatments. Physiologia Plantarum 106: 121–128.
Google Scholar: Author Only Title Only Author and Title

Wenzel, C.L., Williamson, R.E., and Wasteneys, G.O. (2000). Gibberellin-Induced Changes in Growth Anisotropy Precede Gibberellin-Dependent Changes in Cortical Microtubule Orientation in Developing Epidermal Cells of Barley Leaves. Kinematic and Cytological Studies on a Gibberellin-Responsive Dwarf Mutant, M489. Plant Physiology 124: 813–822.
Google Scholar: Author Only Title Only Author and Title

Whitelam, G.C. and Johnson, C.B. (1982). PHOTOMORPHOGENESIS IN IMPATIENS PARVIFLORA AND OTHER PLANT SPECIES UNDER SIMULATED NATURAL CANOPY RADIATIONS. New Phytol 90: 611–618.
Google Scholar: Author Only Title Only Author and Title

Whitelam, G.C. and Smith, H. (1991). Retention of Phytochrome-Mediated Shade Avoidance Responses in Phytochrome-Deficient Mutants of Arabidopsis, Cucumber and Tomato. Journal of Plant Physiology 139: 119–125.
Google Scholar: Author Only Title Only Author and Title

Williams, J., Phillips, A.L., Gaskin, P., and Hedden, P. (1998). Function and Substrate Specificity of the Gibberellin 3β-Hydroxylase Encoded by the Arabidopsis GA4Gene. Plant Physiology 117: 559–563.
Google Scholar: Author Only Title Only Author and Title

Xu, S., Li, L., Luo, X., Chen, M., Tang, W., Zhan, L., Dai, Z., Lam, T.T., Guan, Y., and Yu, G. (2022). Ggtree: A serialized data object for visualization of a phylogenetic tree and annotation data. iMeta 1: e56.
Google Scholar: Author Only Title Only Author and Title

Yamaguchi, S., Smith, M.W., Brown, R.G.S., Kamiya, Y., and Sun Tai-ping (1998a). Phytochrome Regulation and Differential Expression of Gibberellin 3β-Hydroxylase Genes in Germinating Arabidopsis Seeds. The Plant Cell 10: 2115–2126.
Google Scholar: Author Only Title Only Author and Title

Yamaguchi, S., Sun, T., Kawaide, H., and Kamiya, Y. (1998b). The GA2 locus of Arabidopsis thaliana encodes ent-kaurene synthase of gibberellin biosynthesis. Plant Physiology 116: 1271–1278.
Google Scholar: Author Only Title Only Author and Title

Yamane, H. (1998). Fern Antheridiogens. International Review of Cytology 184: 1–32.
Google Scholar: Author Only Title Only Author and Title

Yamaoka, S. et al. (2018). Generative Cell Specification Requires Transcription Factors Evolutionarily Conserved in Land Plants. Current Biology 28: 479-486.e5.
Google Scholar: Author Only Title Only Author and Title

Yamauchi, T., Oyama, N., Yamane, H., Murofushi, N., Schraudolf, H., Pour, M., Furber, M., and Mander, L.N. (1996). Identification of Antheridiogens in Lygodium circinnatum and Lygodium flexuosum. Plant Physiology 111: 741–745.
Google Scholar: Author Only Title Only Author and Title

Yoshida, H., Takehara, S., Mori, M., Ordonio, R.L., and Matsuoka, M. (2020). Evolution of GA metabolic enzymes in land plants. Plant and Cell Physiology 61: 1919–1934.
Google Scholar: Author Only Title Only Author and Title

Yu, G. (2022). Data Integration, Manipulation and Visualization of Phylogenetic Trees (Chapman and Hall/CRC: New York).

Yu, G. (2020a). Gene ontology semantic similarity analysis using GOSemSim. In Methods in Molecular Biology (Humana Press Inc.), pp. 207–215.
Google Scholar: Author Only Title Only Author and Title

Yu, G. (2020b). Using ggtree to Visualize Data on Tree-Like Structures. Current Protocols in Bioinformatics 69: e96.
Google Scholar: Author Only Title Only Author and Title

Yu, G., Lam, T.T.-Y., Zhu, H., and Guan, Y. (2018). Two Methods for Mapping and Visualizing Associated Data on Phylogeny Using Ggtree. Molecular Biology and Evolution 35: 3041–3043.
Google Scholar: Author Only Title Only Author and Title

Yu, G., Li, F., Qin, Y., Bo, X., Wu, Y., and Wang, S. (2010). GOSemSim: an R package for measuring semantic similarity among GO terms and gene products. Bioinformatics 26: 976–978.
Google Scholar: Author Only Title Only Author and Title

Yu, G., Smith, D.K., Zhu, H., Guan, Y., and Lam, T.T.-Y. (2017). ggtree: an r package for visualization and annotation of phylogenetic trees with their covariates and other associated data. Methods in Ecology and Evolution 8: 28–36.
Google Scholar: Author Only Title Only Author and Title

Zhang, Y., Werling, U., and Edelmann, W. (2012). SLiCE: A novel bacterial cell extract-based DNA cloning method. Nucleic Acids Research 40: 1–10.
Google Scholar: Author Only Title Only Author and Title